AGU PUBLICATIONS

JGR

Journal of Geophysical Research: Atmospheres

RESEARCH ARTICLE
10.1002/2014JD022893

Key Points:
- Five-year record of central Andes precipitation isotopic composition
- Precipitation isotopes are elevation dependent, but vary in space and time
- Precipitation isotope variability is related to large-scale climate dynamics

Supporting Information:
- Text S1
- Table S2
- Table S6
- Table S10

Correspondence to:
R. P. Fiorella,
richf@umich.edu

Citation:
Fiorella, R. P., C. J. Poulsen, R. S. Pillco Zolá, J. B. Barnes, C. R. Tabor, and T. A. Ehlers (2015), Spatiotemporal variability of modern precipitation $\delta^{18}O$ in the central Andes and implications for paleoclimate and paleoaltimetry estimates, *J. Geophys. Res. Atmos.*, *120*, 4630–4656, doi:10.1002/2014JD022893.

Received 25 NOV 2014
Accepted 16 APR 2015
Accepted article online 21 APR 2015
Published online 23 MAY 2015

Spatiotemporal variability of modern precipitation $\delta^{18}O$ in the central Andes and implications for paleoclimate and paleoaltimetry estimates

Richard P. Fiorella[1], Christopher J. Poulsen[1], Ramiro S. Pillco Zolá[2], Jason B. Barnes[1,3], Clay R. Tabor[1], and Todd A. Ehlers[4]

[1]Department of Earth and Environmental Sciences, University of Michigan, Ann Arbor, Michigan, USA, [2]Instituto de Hidráulica e Hidrología, Universidad Mayor de San Andrés, Nuestra Señora de La Paz, Bolivia, [3]Now at Landscape Analytics LLC, Raleigh, North Carolina, USA, [4]Institute of Geosciences, University of Tübingen, Tübingen, Germany

Abstract Understanding the patterns of rainfall isotopic composition in the central Andes is hindered by sparse observations. Despite limited observational data, stable isotope tracers have been commonly used to constrain modern-to-ancient Andean atmospheric processes, as well as to reconstruct paleoclimate and paleoaltimetry histories. Here, we present isotopic compositions of precipitation ($\delta^{18}O_p$ and δD_p) from 11 micrometeorological stations located throughout the Bolivian Altiplano and along its eastern flank at ~21.5°S. We collected and isotopically analyzed 293 monthly bulk precipitation samples (August 2008 to April 2013). $\delta^{18}O_p$ values ranged from −28.0‰ to 9.6‰, with prominent seasonal cycles expressed at all stations. We observed a strong relationship between the $\delta^{18}O_p$ and elevation, though it varies widely in time and space. Constraints on air sourcing estimated from atmospheric back trajectory calculations indicate that continental-scale climate dynamics control the interannual variability in $\delta^{18}O_p$, with upwind precipitation anomalies having the largest effect. The impact of precipitation anomalies in distant air source regions to the central Andes is in turn modulated by the Bolivian High. The importance of the Bolivian High is most clearly observed on the southern Bolivian Altiplano. However, monthly variability among Altiplano stations can exceed 10‰ in $\delta^{18}O_p$ on the plateau and cannot be explained by elevation or source variability, indicating a nontrivial role for local scale effects on short timescales. The strong influence of atmospheric circulation on central Andean $\delta^{18}O_p$ requires that paleoclimate and paleoaltimetry studies consider the role of South American atmospheric paleocirculation in their interpretation of stable isotopic values as proxies.

1. Introduction

Stable isotopes in precipitation serve as tracers of modern and past environmental processes. Phase changes through processes including evaporation and condensation unequally partition the stable isotopes of water with the heavier isotopes (^{18}O, ^{2}H or D) favoring the more condensed phase [*Dansgaard*, 1964; *Gat*, 1996]. Progressive condensation from an air parcel leaves the residual vapor and subsequent precipitation along a trajectory more depleted in heavy isotopes. The isotopic composition of precipitation (δ_p) is expressed as the per mil (‰) deviation of the heavy-to-light isotope ratio (R) from the Vienna Standard Mean Ocean Water standard (VSMOW) ($\delta_p = 1000 * (R_p / R_{VSMOW} - 1)$) [*Coplen*, 1996; *Gat*, 1996]. A predictable spatial distribution of δ_p emerges when the factors controlling condensation are well known [*Bowen and Wilkinson*, 2002; *Bowen and Revenaugh*, 2003]. Because δ_p preserves information about hydrologic cycling, it is widely applied to understand modern hydrologic processes [*Rozanski et al.,* 1993; *Vuille and Werner*, 2005; *Liu et al.,* 2010]. Paleoenvironmental reconstructions also use δ_p because several geologic proxy materials preserve δ_p directly (e.g., ice cores) [*Grootes et al.,* 1989; *Thompson et al.,* 1998] or form in equilibrium with δ_p (e.g., pedogenic carbonates) [*Cerling and Quade*, 1993; *Quade et al.,* 2007]. Unfortunately, interpretations of δ_p patterns remain hindered in many regions because local measurements of the spatiotemporal variability of modern δ_p are scarce [e.g., *Lechler and Niemi*, 2012]. One robust trend that is observed on a global scale, however, is a general decrease in δ_p with increased elevation [e.g., *Dansgaard*, 1964; *Siegenthaler and Oeschger*, 1980; *Rozanski et al.,* 1993]. This pattern results from the topographically initiated adiabatic lifting of and rainout from air parcels [*Rowley and Garzione*, 2007]. The rate of isotopic change with elevation is commonly referred to the isotopic lapse rate. Observed isotopic lapse rates at local-to-regional scales are highly variable in space and time [*Blisniuk and Stern*, 2005].

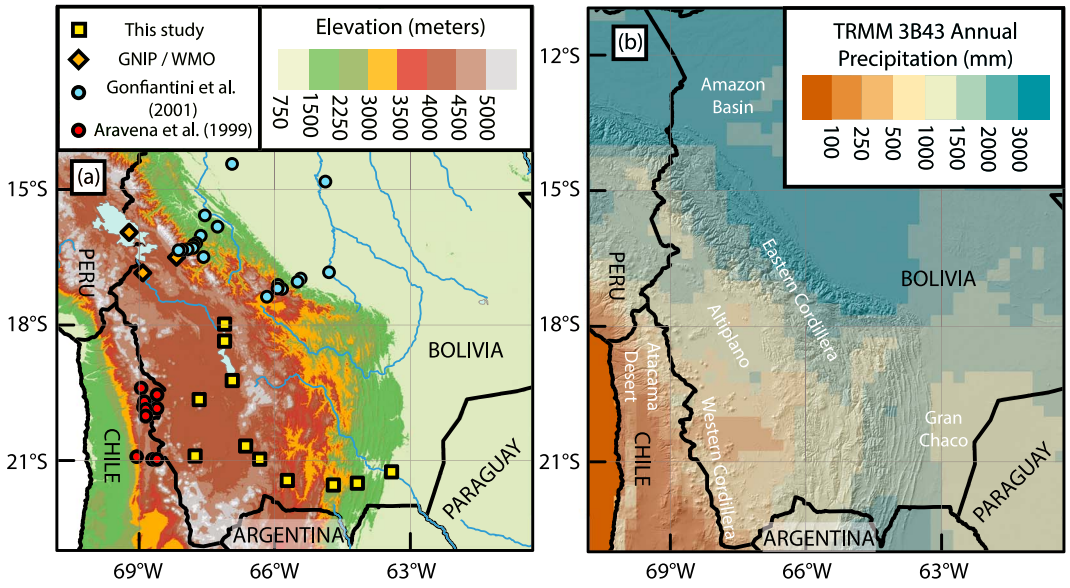

Figure 1. Topography and climatology of the central Andes region: (a) Elevation (m; HydroSHEDS) [*Lehner et al.,* 2008] and relevant climate stations; (b) 1998–2013 mean annual precipitation (MAP; mm/yr) from TRMM 3B43 [*Liu et al.,* 2012]. Prominent topographic features are the broad, flat Altiplano centered between higher peaks to the east and west. Elevation and rainfall gradients are strong in the northeastern flanks of the Altiplano transitioning to weaker gradients east of the southern Altiplano. Precipitation is more seasonal on the Altiplano than in the lowlands.

Despite limited data, stable isotope compositions of natural waters have been widely used to infer (paleo)environmental conditions in the central Andes. Existing observations of precipitation [*Aravena et al.,* 1999; *Gonfiantini et al.,* 2001; *Vimeux et al.,* 2005, 2011] and surface waters [*Hoke et al.,* 2009; *Bershaw et al.,* 2010; *Giovanni et al.,* 2010; *Rohrmann et al.,* 2014] along the flanks of the central Andean plateau (the Altiplano) form the basis of our knowledge of regional water isotopologue distributions (Figure 1a). These observations reveal that the central Andean isotopic distribution and lapse rate varies considerably in space and time. For example, the $\delta^{18}O_p$ lapse rate was −1.9‰/km on the eastern Andean flank from July 1984 to June 1985 [*Gonfiantini et al.,* 2001] compared to approximately −3.3‰/km on the western Andean flank in 1986 [*Aravena et al.,* 1999]. Estimates of the isotopic lapse rate derived from stream waters also vary substantially and range from −1.9‰/km (2004–2005, ~16°S) [*Bershaw et al.,* 2010] to −0.2‰/km (2010–2013, ~26°S) [*Rohrmann et al.,* 2014]. The high observed variability in δ_p is thought to be related to continental-scale climate variability; precipitation anomalies in upwind vapor source regions have been shown to influence eastern Andean flank δ_p values [*Vimeux et al.,* 2005, 2009, 2011; *Vuille et al.,* 2012].

However, key uncertainties about controls on central Andean δ_p remain for several reasons. First, observations are neither broadly distributed, particularly within the Altiplano, nor contemporaneous. Second, existing modern δ_p records are short in duration (<2 years), despite known high interannual variability in central Andean climate [*Garreaud et al.,* 2003, 2009]. Finally, the δ_p data lack a consistent sampling method. Some studies measured δ_p of monthly precipitation [*Gonfiantini et al.,* 2001; *Vimeux et al.,* 2005], while others measured δ_p from individual precipitation events [*Aravena et al.,* 1999; *Vimeux et al.,* 2011]. Thus, it has proven difficult to determine if these limited records represent modern climatological mean conditions, much less how applicable they may be over geologic time [e.g., *Barnes and Ehlers*, 2009].

Climate simulations using isotope-tracking general circulation models have sought to fill the gap of limited δ_p observations and explore how δ_p changes in response to surface uplift, climate change, and different moisture sources [*Vuille et al.,* 2003a, 2003b; *Sturm et al.,* 2007; *Ehlers and Poulsen*, 2009; *Lee et al.,* 2009a; *Insel et al.,* 2010; *Lewis et al.,* 2010; *Poulsen and Jeffery*, 2011; *Insel et al.,* 2012; *Jeffery et al.,* 2012; *Insel et al.,* 2013]. Simulations of modern δ_p confirm a distinct decrease with elevation on the Altiplano margin, yet also predict high interannual variability of δ_p across the entire central Andean region that equals or even exceeds the observed flank δ_p variability [*Sturm et al.,* 2007; *Insel et al.,* 2013]. The simulations demonstrate that salient features of South American atmospheric circulation, such as the upper level (200 hPa) Bolivian High and the South

American Low-Level Jet (SALLJ, 850 hPa), govern the patterns of δ_p, including the steering of air parcels towards the central Andes [*Insel et al.,* 2013]. Upstream precipitation amounts along the parcel trajectories also contributes to δ_p variability [*Vuille et al.,* 2003a, 2003b; *Vuille and Werner*, 2005; *Sturm et al.,* 2007; *Insel et al.,* 2013]. However, observations to validate these simulated large spatiotemporal variations in δ_p remain inadequate.

We present a long (~5 yrs) observational record of δ_p in Andes precipitation to augment our knowledge of central Andes δ_p. We next integrate the isotopic data with climate reanalysis and air parcel back trajectory modeling to evaluate whether previously identified controls on δ_p along the eastern Andean flank extend to the high plateau region. Specifically, we test the hypotheses that: (a) elevation is a dominant control on Altiplano δ_p and (b) Altiplano δ_p inherits variability from precipitation anomalies in distant air source regions, as it does along the flanks. In addition, we measure δ_p along a previously unsampled eastern flank transect at ~21.5°S and compare it to existing studies to investigate the spatial variability in the δ_p-elevation relationship. Finally, we suggest that prior observational records of modern precipitation may be too short in duration to fully sample natural variability. We then use these insights to discuss how improved knowledge of the spatiotemporal patterns of central Andean δ_p may progress interpretation of regional proxies for paleoclimate and paleoelevation.

2. Background

2.1. Central Andes Climate and Topography

Strong elevation and annual precipitation gradients in the central Andes likely influence δ_p. In the central Andes, the range splits into two distinct cordilleras each with ~5 km of relief that bound the interior, low-relief Altiplano (at ~3800 m elevation) (Figure 1). To the west, the Atacama Desert in northern Chile receives less than 20 mm/yr precipitation on average, while in the Amazon Basin to the northeast, mean annual precipitation (MAP) amounts can exceed 5000 mm/yr [*Garreaud et al.,* 2009]. On the Bolivian Altiplano, precipitation amounts range from ~1000 mm/yr in the north (16–18°S) to $<$ 200 mm/yr in the south (20–22°S; Figure 1b). Across the Atacama Desert located on the western flank, hyperarid conditions arise from strong atmospheric subsidence collocated with the cold, coastal Humboldt current [*Rodwell and Hoskins*, 2001; *Takahashi and Battisti*, 2007; *Garreaud et al.,* 2010].

Central Andean climate exhibits a strong seasonal cycle as well. The majority of precipitation occurs during austral summer (compare Figures 2a and 2c to Figures 2b and 2d) [*Garreaud and Aceituno*, 2001; *Garreaud et al.,* 2003]. On the Bolivian Altiplano, the proportion of MAP falling during December-January-February (DJF) often exceeds 60% [*Garreaud et al.,* 2003]. DJF rainfall is typically convective and results from increased moisture convergence that occurs with the development of the Bolivian High [*Lenters and Cook*, 1999] and an increase in SALLJ moisture transport [*Campetella and Vera*, 2002; *Insel et al.,* 2010]. In contrast, arid conditions prevail in the absence of the Bolivian High during June-July-August (JJA) (Figures 2b and 2c).

Precipitation amounts over the Altiplano vary substantially from year to year [*Garreaud and Aceituno*, 2001], perhaps with changes in the position and intensity of the Bolivian High. Strengthening or southward displacement of the Bolivian High both favor increased Altiplano precipitation, while a weaker or more northerly Bolivian High favors decreased Altiplano precipitation [*Lenters and Cook*, 1999; *Garreaud and Aceituno*, 2001]. In addition, the amount of precipitation on the plateau appears related to the state of El Niño/Southern Oscillation (ENSO) [*Thompson et al.,* 1984; *Aceituno*, 1988; *Lenters and Cook*, 1999; *Vuille*, 1999]. Changes in precipitation amount and vapor sourcing through such modes of interannual-to-decadal climate variability likely portend high variability in δ_p.

2.2. Stable Isotope Systematics

The degree of partitioning of water isotopologues (e.g., $H_2{}^{16}O$ versus $H_2{}^{18}O$) during phase changes depends on the local environmental conditions. The saturation vapor pressure of heavier isotopologues of water is slightly lower than for lighter water isotopologues, which promotes a thermodynamic preference for the heavier water isotopologues entering or remaining in the more condensed phase. The degree of partitioning at equilibrium, also called the equilibrium fractionation factor, decreases with increasing temperature [*Majoube*, 1971; *Horita and Wesolowski*, 1994]. Kinetic isotopic fractionation can also occur when two phases cannot attain isotopic equilibrium. A prominent example of kinetic fractionation is evaporation from the ocean surface, where transport of water vapor from the water surface occurs mainly through diffusion and turbulent transport

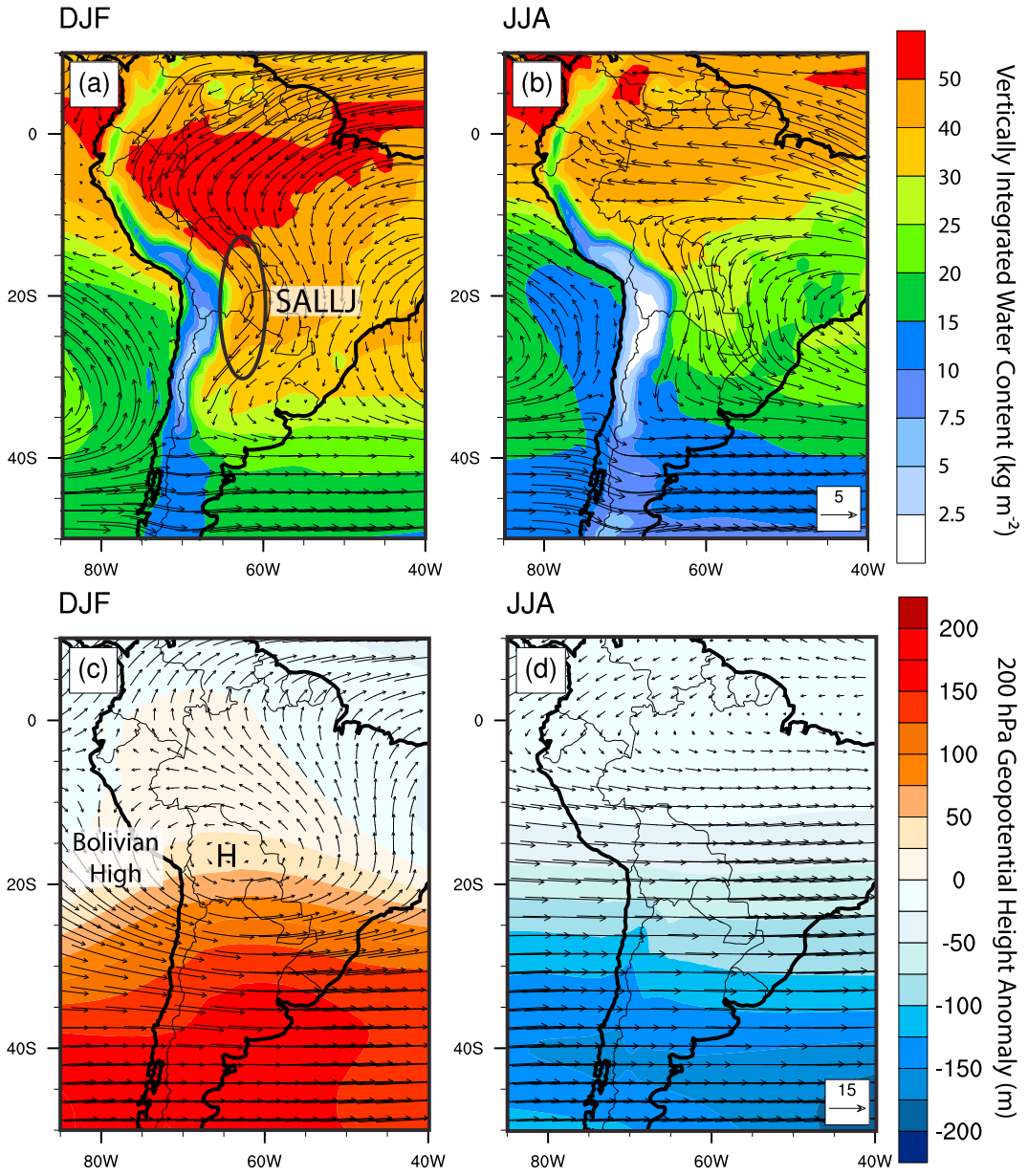

Figure 2. Seasonal climatology for the central Andes from ERA-Interim reanalysis data [*Dee et al.*, 2011]. Climatological (1979–2013) mean 850 hPa winds (vectors, m/s) overlying vertically integrated column water (kg/m^2) for (a) austral summer (DJF) and (b) winter (JJA). Climatological (1979–2013) mean upper level (200 hPa) winds overlying anomalous 200 hPa geopotential height relative to the zonal average for (c) DJF and (d) JJA. Major features of DJF large-scale circulation drive increased moisture convergence to the central Andes like the South American Low-Level Jet (SALLJ, Figure 2a) and the Bolivian High (Figure 2c).

[*Craig and Gordon*, 1965]. The deuterium excess parameter (d-excess $= \delta D_p - 8\delta^{18}O_p$) is seen as a tracer of the kinetic isotope fractionation history of an air parcel and precipitation [e.g., *Dansgaard*, 1964; *Uemura et al.*, 2008].

Following initial evaporation from the ocean, the isotopic composition of precipitation has commonly been explained by Rayleigh distillation [e.g., *Dansgaard*, 1964; *Gat*, 1996]. In a pure Rayleigh system, adiabatic cooling of an air parcel results in condensation occurring in isotopic equilibrium with the remaining vapor. Rayleigh distillation assumes that all condensate is immediately removed and no mixing of vapor occurs between the air parcel and the environment. Continued cooling results in more vapor being removed from the air parcel. Under these conditions, the isotopic composition of an air mass is a function of parcel

temperature during condensation and the fraction of vapor remaining in the air parcel relative to its initial value [*Dansgaard*, 1964; *Gat*, 1996; *Noone*, 2012]:

$$\ln\left(\frac{R}{R_0}\right) = (\alpha_{l\text{-}v}(T) - 1)\ln\left(\frac{w}{w_0}\right) \approx (\delta - \delta_0)$$

where R is the heavy-to-light isotope ratio, $\alpha_{l\text{-}v}(T)$ is the temperature dependent fractionation factor between liquid water and vapor [*Majoube*, 1971; *Horita and Wesolowski*, 1994], w is the water vapor mixing ratio, and a subscript zero indicates initial conditions of the parcel. The isotopic composition of water removed from the parcel at any point during condensation can be calculated using the equilibrium fractionation factor, $\alpha_{l\text{-}v}(T)$:

$$\delta_l = (\delta_v + 1000)\alpha_{l\text{-}v}(T) - 1000$$

where δ_l and δ_v are the isotopic compositions of liquid and vapor, respectively.

The traditional view is that extratropical δ_p obeys Rayleigh distillation to first order [*Dansgaard*, 1964; *Rozanski et al.,* 1993]. Surface and cloud-base temperature both correlate well with δ_p on monthly and annual timescales outside of the tropics, with the strongest correlations observed at high latitudes [*Dansgaard*, 1964; *Rindsberger et al.,* 1983; *Rozanski et al.,* 1993]. In the tropics, however, annual variability in δ_p persists despite more uniform annual temperatures. Instead, δ_p values tend to be lighter during periods of increased precipitation [*Dansgaard*, 1964; *Rozanski et al.,* 1993], and are often negatively correlated with the water vapor content of an air parcel, counter to the Rayleigh distillation relationship [e.g., *Aggarwal et al.,* 2012]. This relationship is referred to as the "amount effect" [*Dansgaard*, 1964; *Rozanski et al.,* 1993].

The amount effect results from multiple convective processes. First, subcloud rainfall evaporation decreases at higher precipitation rates, as droplets tend to be larger and fall faster [*Lee and Fung*, 2007; *Bony et al.,* 2008; *Risi et al.,* 2008]. Subcloud evaporation of rainfall eventually saturates the air column, further suppressing evaporation. Decreased subcloud evaporation of raindrops results in lighter isotopic compositions reaching the surface. Second, convective downdrafts contribute by recycling vapor derived from partial evaporation of raindrops [*Risi et al.,* 2008] and by mixing vapor from the middle-to-upper troposphere down toward the surface that has a lighter isotopic composition than near surface vapor [*Dessler and Sherwood*, 2003; *Kuang et al.,* 2003]. Third, subsidence in large-scale atmospheric circulation can also result in downward mixing of isotopically light vapor [*Blossey et al.,* 2010]. These processes decrease the concentration of heavy isotopologues in surface vapor, resulting in lighter δ_p values when this surface vapor is entrained in subsequent convective updrafts. Finally, more vigorous convection entrains more vapor from the middle-to-upper troposphere, which is isotopically lighter than surface vapor, further contributing to lighter δ_p values in strong convective systems [*Moore et al.,* 2014]. The relative importance of each of these factors likely changes with precipitation rates, with subcloud evaporation dominating at low precipitation rates [*Lee and Fung*, 2007; *Risi et al.,* 2008] and increased importance of vapor recycling and entrainment occurring at higher precipitation rates [*Risi et al.,* 2008; *Moore et al.,* 2014]. Convective precipitation dominates the Amazon basin [*Garreaud et al.,* 2009], and therefore, these processes influence the source vapor for central Andes precipitation.

3. Methods

3.1. Data Collection and Isotopic Analysis Methods

We built a network of eleven micrometeorological stations that collected temperature, relative humidity, and precipitation amounts (Figure 1a). Six stations spanned the Altiplano (18–21°S; 66.5–68°W) and five transected its eastern margin in southern Bolivia at ~21.5°S (E-W; elevations from 395 to 4340 m). The Bolivian meteorological service (SENAMHI) managed four of the Altiplano stations (Oruro, El Choro, Quillacas, and Salinas) and we installed the remaining seven in July 2008 (Figure 3 inset). The meteorological equipment we installed in the stations was manufactured by Onset Computer Corporation. All stations began collecting samples in August 2008. The six Altiplano stations (Oruro, El Choro, Quillacas, Salinas, San Juan, Noel Mariaca) and the highest elevation station along the plateau flank (Gran Chocaya) operated until April 2013. We retired the four remaining stations along the elevation transect (Tupiza, Tarija, Entre Ríos, and Villamontes) at the end of September 2011. At each location, we employed resident observers to maintain the station and collect monthly precipitation samples for subsequent isotopic analysis. Precipitation samples were captured with rain buckets, the inner bottoms of which were covered with a layer of mineral oil to prevent evaporation [after *Friedman et al.,* 1992; *Scholl et al.,* 1996]. On the first of each month, observers collected precipitation

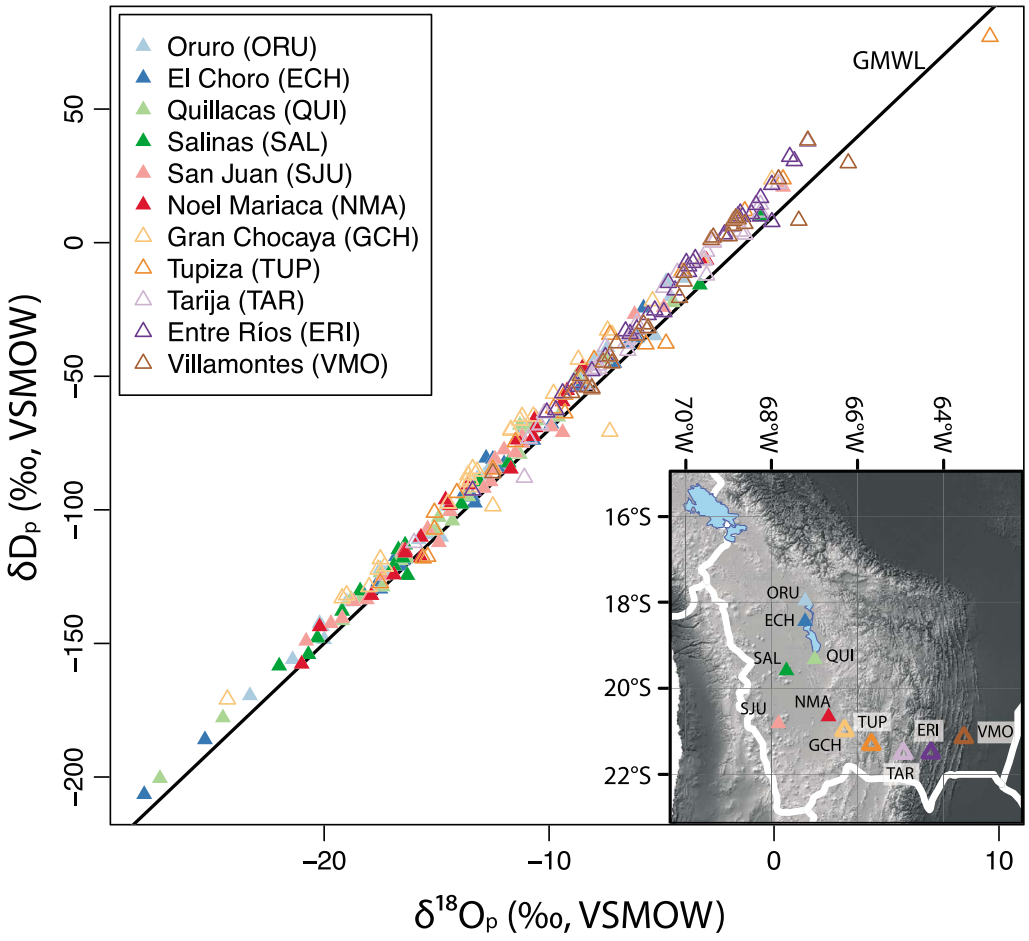

Figure 3. Monthly isotopic composition of precipitation in $\delta^{18}O_p$-δD_p space. Values for all 11 stations in this study are shown as separate colors. GMWL = heavy black line. Inset map shows station locations with symbols (filled = Altiplano stations, open = elevation transect) and colors used throughout the paper.

samples from the bottom of the bucket using a syringe and transferred it to a 20 mL glass vial with poly-cone cap (made by Wheaton). The bucket was then emptied, cleaned, dried, the bottom refilled with mineral oil, and replaced. During semiannual trips to collect the precipitation samples, we interviewed the observers to learn about recent rainfall conditions and confirm that the precipitation was collected correctly.

Upon our visits to the stations, we discovered that equipment had occasionally malfunctioned due to the harsh and remote conditions at the stations. As a result, some meteorological data was lost, and we used several methods to fill in the resulting data gaps. Gaps in relative humidity (46.4% missing) and temperature (32.1% missing) data were filled using the ERA-Interim reanalysis product at native resolution (T255, ~80 km) [*Dee et al.,* 2011] with data from the grid cell overlying the station. Missing temperatures for stations with few missing values were estimated using a least-squares linear regression between reanalysis and available temperatures for that station to calibrate the reanalysis data to each individual station. We used a regional regression technique for the three Altiplano stations where >35% of temperature values were missing: Salinas (100% missing), El Choro (100%), and Quillacas (45.6%). In these cases, we regressed between available station and reanalysis data from the other three Altiplano stations (Oruro, Noel Mariaca, and San Juan), and used this relationship to predict the missing values for Salinas, El Choro, and Quillacas. Missing relative humidity values were estimated using relative humidity values at the lowest available pressure level above the surface pressure. We applied no correction to the ERA-Interim relative humidity values. Missing monthly precipitation values were estimated using the TRMM 3B43 (0.25° resolution) data set for the grid cell overlying the station [*Huffman et al.,* 2007; *Liu et al.,* 2012]. Rain gauges at Noel Mariaca (November 2009 to April 2011) and Villamontes (August 2010 to September 2011) malfunctioned for ~1 year; we filled these

Table 1. Annual Amount-Weighted Mean $\delta^{18}O_p$, Total Precipitation Amount, and Number of Isotopic Samples Collected

	Isotopic Samples Retrieved	Annual			DJF Only		
		Precipitation (mm)	$\delta^{18}O$ (‰)	δD (‰)	Precipitation (mm)	$\delta^{18}O$ (‰)	δD (‰)
		Oruro (ORU, 17.98°S, 67.11°W, 3718 masl)					
Aug 2008 to June 2009	5	331	−15.5	−106.4	223	−14.8	−99.4
July 2009 to June 2010	9	503	−13.7	−92.9	336	−15.9	−110.6
July 2010 to June 2011	8	357	−18.5	−131.5	233	−21.5	−156.1
July 2011 to June 2012	8	482	−16.0	−111.6	319	−15.2	−105.5
June 2012 to April 2013	7	333	−14.1	−96.6	264	−14.5	−99.7
Total/Average	*37*	*2006*	*−15.5*	*−107.1*			
		El Choro (ECH, 18.36°S, 67.11°W, 3706 masl)					
Aug 2008 to June 2009	6	516	−17.9	−125.9	293	−18.4	−129.1
July 2009 to June 2010	8	568	−10.6	−70.7	355	−11.3	−75.6
July 2010 to June 2011	5	623	−19.5	−140.0	408	−23.2	−170.0
July 2011 to June 2012	5	619	−14.7	−103.7	447	−14.2	−99.1
June 2012 to April 2013	0	407	N/A	N/A	333	N/A	N/A
Total/Average	*24*	*2733*	*−15.6*	*−109.2*			
		Quillacas (QUI, 19.23°S, 66.94°W, 3780 masl)					
Aug 2008 to June 2009	5	233	−16.3	−112.9	183	−15.9	−110.0
July 2009 to June 2010	8	296	−11.6	−78.2	208	−12.6	−85.1
July 2010 to June 2011	6	494	−19.4	−139.1	285	−21.7	−158.1
July 2011 to June 2012	7	359	−16.6	−118.5	283	−16.2	−114.3
June 2012 to April 2013	2	416	−11.9	−77.5	350	−11.9	−77.4
Total/Average	*28*	*1798*	*−15.5*	*−108.1*			
		Salinas (SAL, 19.65°S, 67.64°W, 3719 masl)					
Aug 2008 to June 2009	6	232	−20.6	−145.3	130	−16.8	−117.7
July 2009 to June 2010[a]	5	237	−8.7	−61.0	138	−15.0	−105.8
July 2010 to June 2011[a]	5	241	−18.2	−101.6	172	−19.3	−138.7
July 2011 to June 2012[a]	3	322	−20.7	−154.1	234	−20.7	−154.1
June 2012 to April 2013	0	244	N/A	N/A	202	N/A	N/A
Total/Average	*19*	*1276*	*−17.5*	*−122.6*			
		San Juan (SJU, 20.90°S, 67.76°W, 3663 masl)					
Aug 2008 to June 2009	5	64	−15.8	−111.5	27	−10.5	−71.9
July 2009 to June 2010	6	119	−13.1	−91.9	101	−13.4	−94.5
July 2010 to June 2011	5	169	−15.1	−106.0	154	−15.1	−106.1
July 2011 to June 2012	5	270	−13.9	−98.5	180	−15.0	−104.8
June 2012 to April 2013	3	190	−14.1	−95.2	133	−14.1	−95.2
Total/Average	*24*	*812*	*−14.3*	*−99.8*			
		Noel Mariaca (NMA, 20.68°S, 66.64°W, 3780 masl)					
Aug 2008 to June 2009	4	124	−15.9	−114.0	92	−15.5	−110.5
July 2009 to June 2010	4	148	−8.9	−54.6	112	−8.7	−52.1
July 2010 to June 2011	4	159	−14.4	−104.3	110	−14.4	−106.4
July 2011 to June 2012	5	256	−15.2	−106.0	212	−15.1	−104.5
June 2012 to April 2013	3	160	−14.9	−100.2	141	−14.9	−100.2
Total/Average	*20*	*847*	*−14.1*	*−97.8*			
		Gran Chocaya (GCH, 20.97°S, 66.33°W, 4340 masl)					
Aug 2008 to June 2009	5	233	−13.2	−81.1	147	−14.3	−89.7
July 2009 to June 2010	7	255	−13.8	−89.4	208	−14.8	−97.3
July 2010 to June 2011	4	216	−13.6	−96.4	163	−13.3	−96.4
July 2011 to June 2012	7	246	−14.7	−97.8	167	−15.4	−102.0
June 2012 to April 2013	5	186	−14.4	−93.2	157	−14.6	−95.0
Total/Average	*28*	*1136*	*−14.0*	*−92.0*			
		Tupiza (TUP, 21.44°S, 65.72°W, 2974 masl)					
Aug 2008 to June 2009	7	476	−9.1	−51.2	361	−8.8	−48.3
July 2009 to June 2010	6	243	−11.2	−74.0	215	−11.7	−78.1
July 2010 to June 2011	6	203	−13.0	−90.0	162	−13.0	−89.6
Total/Average	*19*	*922*	*−10.5*	*−65.8*			

Table 1. (continued)

	Isotopic Samples Retrieved	Annual			DJF Only		
		Precipitation (mm)	$\delta^{18}O$ (‰)	δD (‰)	Precipitation (mm)	$\delta^{18}O$ (‰)	δD (‰)
		Tarija (TAR, 21.54°S, 64.70°W, 1884 masl)					
Aug 2008 to June 2009	11	718	−5.3	−22.8	396	−5.4	−22.4
July 2009 to June 2010	9	686	−8.8	−55.1	496	−9.8	−63.4
July 2010 to June 2011	8	460	−9.8	−62.8	331	−10.1	−65.7
Total/Average	*29*	*1864*	*−7.7*	*−44.5*			
		Entre Ríos (ERI, 21.50°S, 64.17°W, 1261 masl)					
Aug 2008 to June 2009	11	860	−5.7	−26.0	429	−5.2	−22.2
July 2009 to June 2010	11	774	−7.1	−40.0	425	−8.5	−51.8
July 2010 to June 2011	12	631	−9.0	−55.6	477	−9.7	−61.9
Total/Average	*36*	*2265*	*−7.0*	*−38.9*			
		Villamontes (VMO, 21.25°S, 63.41°W, 395 masl)					
Aug 2008 to June 2009	8	630	−5.4	−25.4	351	−5.3	−25.6
July 2009 to June 2010	9	489	−7.2	−45.6	339	−8.2	−54.3
July 2010 to June 2011	10	793	−7.9	−46.7	597	−8.8	−54.2
Total/Average	*29*	*1912*	*−6.8*	*−39.0*			

[a]Some samples during these periods did not meet quality checks and were not included in these analyses.

gaps with TRMM data as well. Because we could not be certain when the rain gauges first malfunctioned, we assumed they stopped operating when the data diverged from nearby stations or TRMM data. We estimate that average TRMM-derived precipitation values are within ~25% of measured values (Figure S1 and Table S1). Precipitation amounts are underestimated by ~25% by TRMM relative to station measurements for the transect stations, while Altiplano stations are overestimated by ~15% on average (Table S1). However, TRMM overestimates precipitation at the Noel Mariaca and Gran Chocaya stations by ~38% and 23% respectively, relative to available station measurements (Table S1). We provide the monthly micrometeorological data in Table S2 and indicate the points derived from ERA-Interim or TRMM for transparency.

We analyzed the precipitation isotopic compositions using a Picarro L2120-i cavity ringdown spectrometer with an integrated A211 high-precision vaporizer and autosampler. The Picarro ChemCorrect software package monitored samples for organic contamination [e.g., *West et al.,* 2011]. Standard errors are < 0.1‰ for $\delta^{18}O$ and < 0.4‰ for δD. We report the raw monthly data for our 11 stations in Table S2, and annual and DJF average values in Table 1. As the rainy season occurs across two calendar years, we calculated annual averages using a 12 month period from July to June instead of January to December. This method improves representation of the central Andes hydrologic year, and therefore better isolates sources of interannual variability by keeping whole rainy season periods intact.

A strong correlation between $\delta^{18}O_p$ and δD_p forms the basis for the global meteoric water line (GMWL, $\delta D_p = 8\delta^{18}O_p + 10$) [*Craig*, 1961]. The GMWL describes the coevolution of water isotopologues as rainout from an air parcel occurs. On local and regional scales, deviations from the GMWL can occur due to local climate conditions [e.g., *Rozanski et al.,* 1993]. We calculated annual, DJF, and JJA local meteoric water lines for each station (Table S3). We found the relationship between $\delta^{18}O_p$ and δD_p is similar for all stations on an annual and DJF basis (Figure 3), but can vary substantially in JJA. For brevity, however, we focus the bulk of the analysis on the $\delta^{18}O_p$ values, as analyzing δD_p on an annual or rainy season basis yields near similar results. JJA variability in the local meteoric water lines is briefly discussed in the results.

We removed 11 monthly values at the Salinas station from the analysis because they failed our data quality criteria, which we attribute to observer error. Four were eliminated for exhibiting substantial evaporation (i.e., negative *d*-excess values) not observed in other samples, and seven samples from the dry season for having identical δ values. We infer that these samples are likely from groundwater or tap water provided by the observer rather than precipitation (indicated in Table S2).

3.2. Data Analysis and Statistical Methods

We performed a suite of multivariate least-squares linear regressions to assess the influence of climatic and geographic factors on $\delta^{18}O_p$ (Table S4). We first determined the best fit model for our stations, then repeated

Table 2. Correlation Coefficient Matrix Comparing the $\delta^{18}O_p$ Timeseries for All Stations[a]

	El Choro	Quillacas	Salinas	San Juan	Noel Mariaca	Gran Chocaya	Tupiza	Tarija	Entre Ríos	Villamontes
Oruro	**0.734**	**0.745**	**0.631**	*0.357*	0.044	**0.676**	**0.805**	**0.746**	**0.754**	**0.641**
El Choro		**0.855**	0.413	0.214	**0.702**	**0.753**	**0.778**	0.386	**0.665**	**0.659**
Quillacas			0.354	**0.537**	**0.564**	**0.645**	**0.826**	0.383	**0.669**	**0.743**
Salinas				0.460	0.238	**0.641**	**0.642**	*0.463*	**0.555**	0.444
San Juan					0.240	**0.504**	**0.741**	0.224	0.283	0.237
Noel Mariaca						**0.536**	0.441	−0.223	0.346	0.294
Gran Chocaya							**0.828**	*0.480*	**0.604**	**0.666**
Tupiza								**0.658**	**0.809**	**0.755**
Tarija									**0.711**	**0.742**
Entre Ríos										**0.786**

[a]Relationships that are significant at the $p = 0.05$ level are bolded and those at the $p = 0.10$ level are italicized.

the regression calculations including monthly bulk $\delta^{18}O_p$ data from prior precipitation studies in the central Andes (hereafter, referred to as all available data) [*Aravena et al.,* 1999; *Gonfiantini et al.,* 2001; *WMO/IAEA*, 2013]. We calculated precipitation amount-weighted annual average $\delta^{18}O_p$ values where monthly precipitation amounts were available. Predictor variables that may modify $\delta^{18}O_p$ include station elevation, latitude, longitude, MAP, and mean annual temperature (MAT) [*Bowen and Wilkinson*, 2002; *Bowen and Revenaugh*, 2003; *Lechler and Niemi*, 2012]. We note that latitude and longitude are not processes that fractionate water isotopologues directly, but they do represent the combined effects of multiple factors that influence their distribution, such as temperature or distance from monsoon circulations. As observational records of $\delta^{18}O_p$ are not contemporaneous, we standardized estimates of MAP and MAT to a common observational data source and reference time period. We extracted MAP and MAT for each station using the University of Delaware 0.5° gridded monthly climate data set (1960–1990 average) [*Legates and Willmott,* 1990a, 1990b]. However, after compilation we observed that several predictor (i.e., independent) variables strongly covaried. Thus, in our multivariate regressions, we excluded MAT and longitude as predictor variables, as they are highly correlated with elevation in our data set (our stations: $r = -0.920$ and -0.918; all available data: $r = -0.740$ and -0.611). However, we retain the potential influence of zonal average temperature changes with latitude by including latitude as a predictor variable. MAP is also strongly correlated with elevation (our stations: $r = -0.861$; all available data: $r = -0.717$), but we retain MAP as a possible predictor variable here due to the strong influence precipitation amount can have on $\delta^{18}O_p$ through the amount effect in the tropics [*Dansgaard*, 1964; *Rozanski et al.,* 1993]. We then used the small-sample Akaike Information Criterion (AICc) to select the best multivariate model because it optimizes the trade-off between model complexity and quality of the fit [*Burnham and Anderson*, 2002]. Low AICc scores signal a multivariate model more parsimonious with the data.

We calculated correlation coefficients (Pearson's r) and *p*-values for all possible station pairs to access the spatial coherence in observed variability across our stations (Table 2). High *r*-values ($>$ ~0.5) between two stations indicate a high likelihood that similar factors affect $\delta^{18}O_p$ at both. We used monthly average outgoing longwave radiation (OLR) from the ERA-Interim reanalysis data set as a proxy for deep convection and high cloud tops [*Kousky*, 1988; *Xie and Arkin*, 1998]. Low values of OLR indicate high cloud tops and deep convective activity.

3.3. Atmospheric Back Trajectory Modeling

To constrain moisture source directions, we calculated 7 day air parcel back trajectories for the rainy season (DJF only) using the HYSPLIT4 model (HYbrid Single-Parcel Lagrangian Integrated Trajectory 4; hereafter HYSPLIT). HYSPLIT model algorithms are well documented [*Draxler and Hess*, 1998], and they have been applied to demonstrate links between $\delta^{18}O_p$ and air transport pathways [e.g., *Strong et al.,* 2007; *Bershaw et al.,* 2012; *Lechler and Galewsky*, 2013]. We modeled air parcel three-dimensional motion using the ERA-Interim reanalysis winds. The ERA-Interim data set has a horizontal resolution of approximately ~80 km [*Dee et al.,* 2011], resulting in a more realistic representation of Andean topography with smaller topographic truncation errors than prior reanalysis products. We initiated back trajectories at a height of 1500 m above ground level at five different station coordinates: Oruro, Quillacas, and Noel Mariaca to represent the northern, central, and southern Bolivian Altiplano respectively, and Tarija and Villamontes to represent the eastern flank (Figure 3). We started at 1500 m above ground level because it reflects a balance between being low enough to be important for moisture transport yet high enough to reduce atmospheric flow attenuation by surface friction

[e.g., *Bershaw et al.,* 2012]. Sensitivity tests using initial heights of 500, 1000, and 2000 m (not shown) resulted in qualitatively similar results to those presented here at 1500 m. We calculated trajectories every 6 h during the rainy season (DJF), resulting 360 total trajectories (364 for leap years) per station per year.

We calculated areal mean frequencies for three prominent 2°×4° source pathways to more quantitatively evaluate the partitioning of DJF air sources emerging from back trajectory modeling. Three regions capture most of the transport to the central Andes: (a) the Yungas-Amazon Basin (YAB) (13–15°S, 65–69°W), (b) the South Pacific (SP) (20–24°S, 69–71°W), and (c) the Gran Chaco (GC) (24–26°S, 62–66°W). We binned hourly parcel position counts from the HYSPLIT back trajectories on a 0.75° grid, then used them to calculate the percentage of trajectories that pass through each 0.75° grid cell. We focused on DJF because this period captures the majority of annual precipitation for all stations (Table 1), and thus, largely determines annual weighted $\delta^{18}O_p$. We normalized the partitioning of air transport from these three regions to 100% to compare between the three main source regions more directly. Nonnormalized trajectory partitioning values are provided in the supporting information (Tables S5 and S6).

To assess the sensitivity of our results to the HYSPLIT data source used, we also calculated back trajectories using the NCEP/NCAR reanalysis data set. We found that air transport patterns with the NCEP/NCAR reanalysis are qualitatively similar to those calculated from ERA-Interim data, though with less advection from the South Pacific region (Figure S2 and Table S7). We attribute these changes to resolution differences between the two reanalysis data sets: NCEP/NCAR is ~2.5° while ERA-Interim is ~0.75°. We therefore consider results from the ERA-Interim data set to more accurately represent the influence of regional topography on air source pathways.

3.4. Data Caveats

We acknowledge our analyses are subject to two major limitations. First, the isotopic data represent point measurements, yet the reanalysis products we used are gridded values averaged over much larger areas. Fortunately, the recent release of high-resolution reanalysis products reduces the severity of this problem [*Dee et al.,* 2011]. Regardless, resolutions remain at ~50–75 km and many key precipitation processes occur on smaller spatial scales (~1–10 km). Thus, simulated precipitation amounts depend highly on the choice of model parameterizations [*Grell*, 1993; *Zhang and McFarlane*, 1995]. Second, TRMM precipitation amounts inferred from continental deep convective systems are uncertain [*Iguchi et al.,* 2009; *Rasmussen et al.,* 2013]. Precipitation variability within the TRMM radar footprint also tends to underestimate rainfall amounts in deep convective systems [*Iguchi et al.,* 2009]. However, these studies used the TRMM 2A25 product, which relies on TRMM precipitation radar measurements only. The TRMM 3B43 product we used reduces the potential satellite bias by incorporating surface observations [*Huffman*, 1997; *Huffman et al.,* 2007]. Due to the variable distribution of meteorological stations, however, the bias reduction is also spatially variable. Therefore, though our monthly precipitation estimates for missing values are reasonable when compared to nearby stations, they are likely still biased. We have estimated the bias at each station by regressing station measurements against TRMM values; recall we find it to be $< 25\%$ (see section 3.1, Figure S1, and Table S1). This bias could contribute to the anomalously low observed correlations between precipitation and $\delta^{18}O_p$ at the stations most reliant on the TRMM data (El Choro, Quillacas, and Salinas) relative to the other stations. Additionally, we avoided making quantitative comparisons between upwind precipitation anomalies and central Andean $\delta^{18}O_p$ due to the uncertain size of this TRMM bias. As this bias affects all measurements, we maintain that the sign of the precipitation anomalies observed is more likely to be robust than their magnitudes.

4. Results

All our stations show annual- and DJF-scale relationships between $\delta^{18}O_p$ and δD_p that are close to the GMWL (Figure 3 and Table S3). This indicates that the annual and DJF relationships between $\delta^{18}O_p$ and δD_p do not vary systematically in space or time in our data set. Seasonal variations during JJA result in markedly different local meteoric water lines (Table S3) that are associated with high *d*-excess values (Table S8). High *d*-excess observed in these samples likely results from two different effects during the dry season. First, changes in vapor sourcing to the region, such as increased advection from the middle to high latitudes over the ocean, would transport higher *d*-excess vapor to the central Andes resulting from increased kinetic fractionation at the oceanic source [*Uemura et al.,* 2008]. Second, large-scale subsidence during the dry season can mix high *d*-excess vapor from higher in the troposphere down toward the surface [e.g., *Blossey et al.,* 2010; *Samuels-Crow*

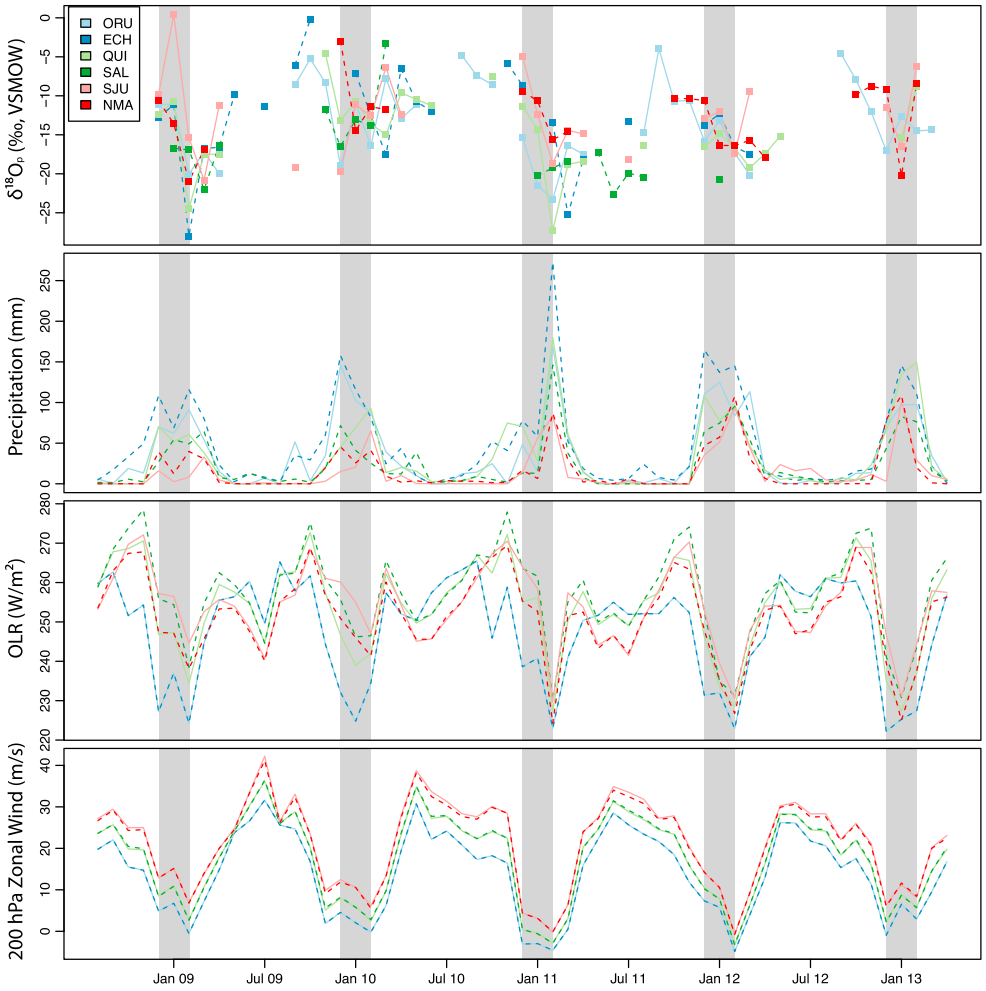

Figure 4. Time series for Altiplano stations of monthly (a) $\delta^{18}O_p$ (‰), (b) precipitation amount (mm), (c) outgoing longwave radiation (OLR, W/m^2), and (d) 200 hPa zonal wind (U, m/s). Missing values in Figure 4a are months where no precipitation was recorded or no sample was retrieved from the observer. Values in Figures 4c and 4d were calculated from the ERA-Interim reanalysis data set. Missing values in Figure 4b are filled using the TRMM 3B43 data set (see Table S2). The rainy season (DJF) is highlighted in gray columns. Note the strong seasonal cycling across all variables. High precipitation and low $\delta^{18}O$ are associated with OLR and zonal wind minimums.

et al., 2014b]. However, as central Andes JJA precipitation represents a small fraction (<10%) of the annual total, we focus the following analysis on $\delta^{18}O_p$ for brevity because analyzing δD_p yields near identical results.

Central Andes monthly $\delta^{18}O_p$ varies considerably across annual to seasonal timescales. Values ranged from −28.0‰ (El Choro, February 2009, Figure 4a) to 9.6‰ (Tupiza, September 2011, Figure 5a). Plateau $\delta^{18}O_p$ values were generally more negative than along the eastern flank (compare Figures 4a and 5a). All 11 of our stations exhibited seasonal variability in $\delta^{18}O_p$. The most negative $\delta^{18}O_p$ values occurred during the rainy season (DJF), as more than two thirds of rainy season average $\delta^{18}O_p$ values were more negative than the annual average (Table 1). In contrast, the least negative $\delta^{18}O_p$ values occurred during the dry season (JJA). Gaps in our $\delta^{18}O_p$ records correspond to periods where no precipitation was recorded (Figures 4a and 5a). The plateau stations tended to experience longer dry periods, and therefore, possessed more discontinuous $\delta^{18}O_p$ records (Figure 4a). In addition, plateau stations exhibited larger amplitude seasonal differences between DJF minimum and JJA maximum $\delta^{18}O_p$ values than the flank stations (10–15‰ versus 5–10‰, compare Figures 4a and 5a).

Annual minimums in $\delta^{18}O_p$ occurred in conjunction with annual precipitation maximums, annual OLR minimums, and annual minimums in 200 hPa zonal winds (Figures 4 and 5). Plateau annual precipitation amounts ranged from 64 mm to 623 mm (Table 1), with a maximum measured monthly value of 180 mm

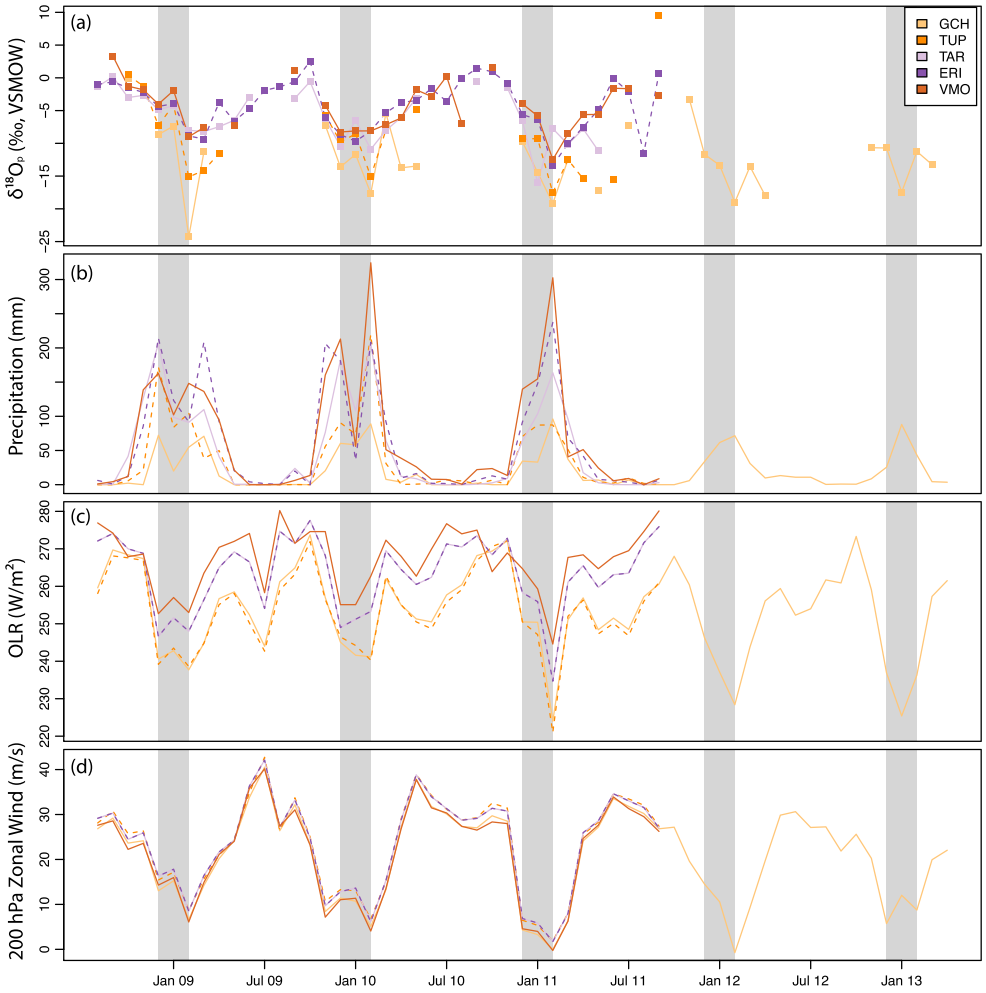

Figure 5. Time series for eastern flank stations of monthly (a) $\delta^{18}O_p$ (‰), (b) precipitation amount (mm), (c) outgoing longwave radiation (OLR, W/m^2), and (d) 200 hPa zonal wind (U, m/s). Missing values in Figure 5a are months where no precipitation was recorded or no sample was retrieved from the observer. Values in Figures 5c and 5d were calculated from the ERA-Interim reanalysis data set. Missing values in Figure 5b are filled using the TRMM 3B43 data set (see Table S2). The rainy season (DJF) is highlighted in gray columns. Note the strong seasonal cycling across all variables. High precipitation and low $\delta^{18}O$ are associated with OLR and zonal wind minimums.

(Quillacas, February 2011) or, if remote-sensed TRMM data are included, 273 mm (El Choro, February 2011) (Figure 4b and Table S2). Flank annual precipitation amounts ranged from 186 mm (Gran Chocaya, July 2012 to June 2013) to 860 mm (Entre Ríos, 11 months, August 2008 to June 2009) (Table 1). Measured monthly values on the flank ranged from 0 mm (various) to 214 mm (Entre Ríos, December 2008), or 324 mm (Villamontes, February 2010) including TRMM estimates (Figure 5b and Table S2). The percentage of annual rain received at each station during DJF ranged from 67 to 78% (El Choro and Noel Mariaca, respectively) on the plateau and 59 to 80% on the flanks (Entre Ríos and Tupiza).

OLR values also exhibited a prominent seasonal cycle characterized by minimum values during DJF, indicating summer convection and increased cloud cover (Figures 4c and 5c). Monthly plateau and flank values had similar ranges; plateau values ranged from 222 W/m^2 (Oruro and El Choro, December 2012) to 279 W/m^2 (Salinas, November 2008) (Figure 4c), and flank values ranged from 221 W/m^2 (Tupiza, February 2011) to 280 W/m^2 (Villamontes, August 2009) (Figure 5c). However, there is a prominent difference in amplitude of the seasonal cycle between the plateau and flank regions. Plateau annual OLR variability can exceed 40 W/m^2 whereas along the flank it is closer to 20–30 W/m^2 (Figures 4d and 5d). The lone exception is Gran Chocaya, which exhibits an annual cycle more similar to plateau stations, though it is located in the high Cordillera adjacent to the plateau.

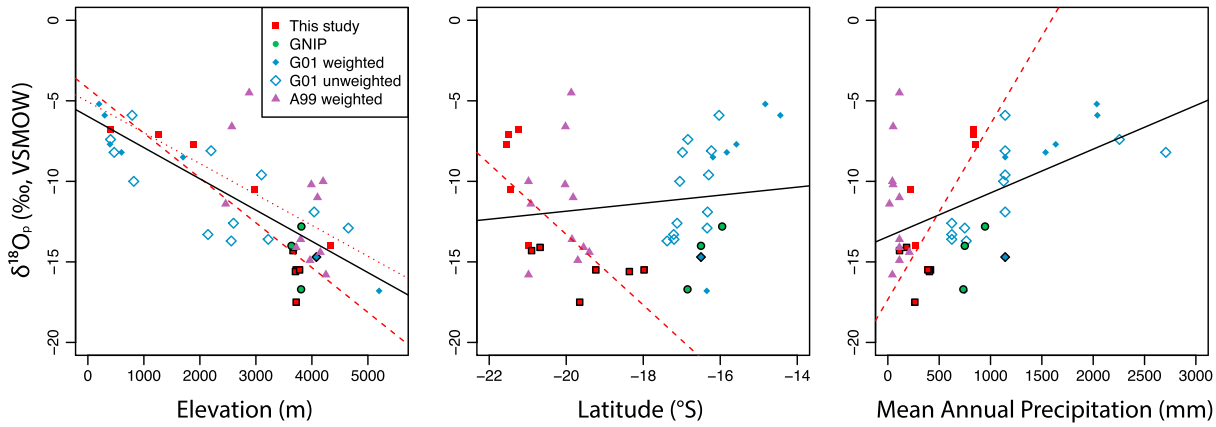

Figure 6. Scatterplots relating weighted annual mean $\delta^{18}O_p$ with (a) elevation, (b) latitude, (c) and mean annual precipitation (MAP) for the central Andes. Red squares are data from our 11 study area stations, purple triangles are data from *Aravena et al.* [1999], filled (open) blue diamonds are weighted (unweighted) data from *Gonfiantini et al.* [2001], and green circles are data from the GNIP stations. Values outlined in black are stations on the plateau. Dashed red line is the best fit linear relationship between $\delta^{18}O_p$ and the predictor variable for stations from this study only, while the solid black line is the best fit linear relationship using all data sources. An additional dotted regression line in Figure 6a excludes the six plateau stations.

The annual cycle of upper level zonal winds mirrors the annual cycle in OLR. During JJA, westerly winds prevail across both the plateau and its flank (Figures 4d and 5d). DJF wind speeds are slower and can be either easterly or westerly. Monthly average upper level zonal wind speeds fluctuate by ~40 m/s across all stations throughout the year. Wind speeds vary spatially on the plateau by ~10 m/s throughout the annual cycle, with consistently greater westerly wind speeds observed in the southern plateau (Figure 4d). In contrast, little variability in upper level wind speeds occurs across flank stations (Figure 5d).

The central Andes annual $\delta^{18}O_p$ variations correspond to cycles of monthly precipitation, OLR, and upper level wind speed, indicating that $\delta^{18}O_p$ responds to seasonal changes in synoptic circulation. Despite these relationships, however, significant spatial, interannual, and month-to-month variability exists in $\delta^{18}O_p$ that cannot be explained solely by these environmental variables. In the following sections, we examine the dominant spatial controls on $\delta^{18}O_p$ and use reanalysis data and back trajectory modeling to identify sources of spatiotemporal variability.

4.1. Relationships Between $\delta^{18}O_p$, Topography, and Climate

Linear regression indicates elevation is the strongest single predictor of $\delta^{18}O_p$ for our stations ($r = -0.907$), as well as for all available data ($r = -0.773$) (Figure 6a). Weaker relationships exist between $\delta^{18}O_p$ and our stations and across all available data for latitude ($r = -0.736$ and 0.147, Figure 6b) and MAP ($r = 0.783$ and 0.496, Figure 6c). Multiple studies have indicated, however, that $\delta^{18}O_p$ can depend on multiple spatial or climatic variables [e.g., *Dansgaard*, 1964; *Bowen and Wilkinson*, 2002; *Lechler and Niemi*, 2012]. Therefore, we tested possible combinations of latitude, elevation, and MAP predictor variables to determine the best multivariate model.

The lowest AICc score shows that the best model for our stations retains elevation and latitude predictors (Table S4). Removing either of these predictor variables increases the AICc score and reduces the goodness of model fit. In contrast, the best AICc model for the entire available data set retains only the elevation predictor (Table S4). However, the AICc score neglects any potential correlation between predictor variables. High correlations between these three predictor variables can be problematic for our multivariate regression models. Elevation and MAP correlate highly for both data sets ($r = -0.861$ stations from this study, $r = -0.717$ for the entire data set). Depending on which data set is used, correlations between latitude and elevation ($r = 0.531$ stations from this study, $r = -0.319$ for the entire data set) and latitude and MAP ($r = -0.277$ stations from this study, $r = 0.717$ for the entire data set) can also be high. As a result, the best fit model should retain only one of these predictor variables. We propose that the best model for our stations includes only elevation because it has the highest univariate correlation with $\delta^{18}O_p$ (Table S4). Furthermore, in both cases, modeled relationships between $\delta^{18}O$ and latitude or MAP are weak and highly sensitive to data subsetting, indicating that neither predictor is a strong regional control on $\delta^{18}O_p$ (Figures 6a and 6b). Despite this apparent control of elevation on $\delta^{18}O_p$ across multiyear timescales,

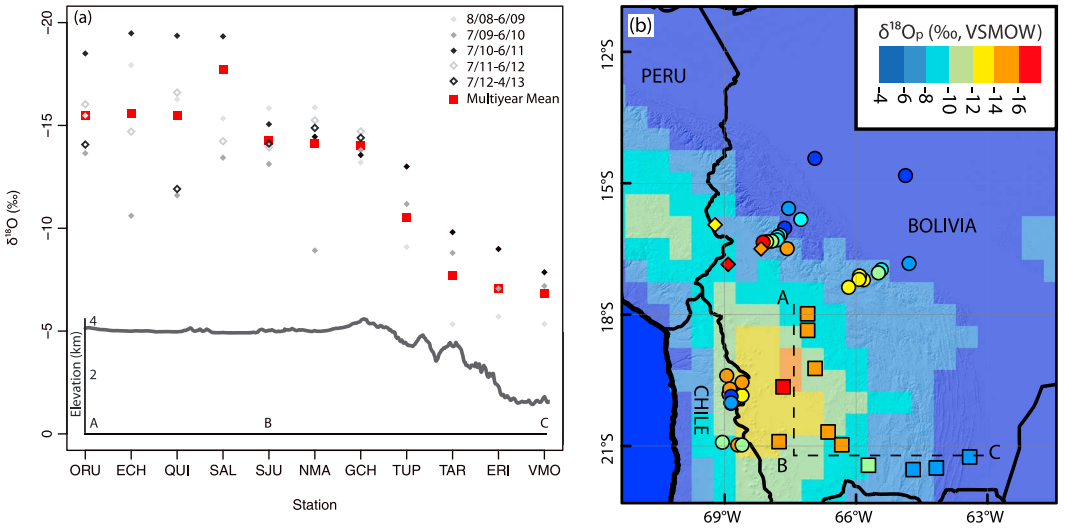

Figure 7. Spatiotemporal variability in central Andes annual mean weighted $\delta^{18}O_p$. (a) All study area stations (unit is ‰, VSMOW). Individual year values are in black/gray symbols, and station mean values are in solid red squares. Along the elevation transect (B–C), interannual variability is twice the magnitude at the low elevation stations than at the highest elevation station. Interannual variability in stations on the Altiplano is much larger than interannual variability along the elevation transect. A swath topographic profile representing local topography is shown below the isotopic values. (b) All available central Andes data. Averages from this study are squares, GNIP stations are diamonds, and data from *Aravena et al.* [1999] and *Gonfiantini et al.* [2001] are circles in Chile and Bolivia, respectively. Symbol fill color indicates the average $\delta^{18}O_p$, with red (blue) values showing more (less) depleted $\delta^{18}O_p$ values. Background contours indicate 10 year amount-weighted annual mean $\delta^{18}O_p$ simulated by the REMOiso regional climate model [*Insel et al.,* 2013, model years 1989–1998].

however, elevation is a poor predictor of $\delta^{18}O_p$ on the Altiplano itself (Figure 6a), and the $\delta^{18}O_p$-elevation relationship is highly variable in space and time.

4.2. Spatial Variability of $\delta^{18}O_p$ and Air Sources

We observe a strong $\delta^{18}O_p$-elevation relationship across our elevation transect (Figure 6a). Amount-weighted $\delta^{18}O_p$ decreases with increasing elevation; the lowest elevation site has an amount-weighted annual average $\delta^{18}O_p$ composition of −6.7‰ (Villamontes, 395 masl) and the highest elevation site −14.0‰ (Gran Chocaya, 4340 masl). For the entire study period, the isotopic lapse rate (defined as the slope of the elevation-$\delta^{18}O_p$ relationship) along this transect was -1.9 ± 0.3‰/km, but ranged from -2.1 ± 0.5‰/km in 2008–2009 to -1.6 ± 0.2‰/km in 2010–2011 (Table S9). These compositions and isotopic lapse rates are comparable to those further north along the eastern Altiplano flank [*Gonfiantini et al.,* 2001]. The northernmost transect (Yungas-Altiplano, centered at ~15°S) in *Gonfiantini et al.* [2001] possessed isotopic lapse rates of -2.1 ± 0.5‰/km and -1.9 ± 0.2‰/km for July 1983 to June 1984 and July 1984 to June 1985, respectively. The Chaparé-Cochabamba transect (centered at ~17°S) in *Gonfiantini et al.* [2001] exhibited an isotopic lapse rate of -1.6 ± 0.2‰/km in 1985 (calendar year, location in Figure 1a). Calendar year and hydrologic (i.e., July to June) year isotopic lapse rates are similar (Table S9). Our isotopic lapse rates are comparable with *Gonfiantini et al.* [2001], though unlike their study, we find no robust relationship between the isotopic lapse rate and precipitation amount. Finally, when combining our data with *Gonfiantini et al.* [2001], we cannot determine if the isotopic lapse rate varies along the length of the eastern flank as estimates from different portions of the flank overlap within error. However, we document that isotopic lapse rates vary by up to ~1.0‰/km from year to year along our plateau flank transect.

Several modes of spatial variability arise in Altiplano $\delta^{18}O_p$ that are not accounted for by the common empirically derived isotopic lapse rates. First, values for all our Altiplano stations (Figure 1a) are more negative than (a) predicted for their elevation (Figure 6a) and (b) the values observed at the upwind, but higher-elevation Gran Chocaya station along the eastern Altiplano margin (0.1–3.6‰ more negative, despite elevations 500 m lower, Figure 7). This trend toward more negative $\delta^{18}O_p$ values indicates that heavy water isotopologues in air parcels on the Altiplano continue to be removed following their ascent

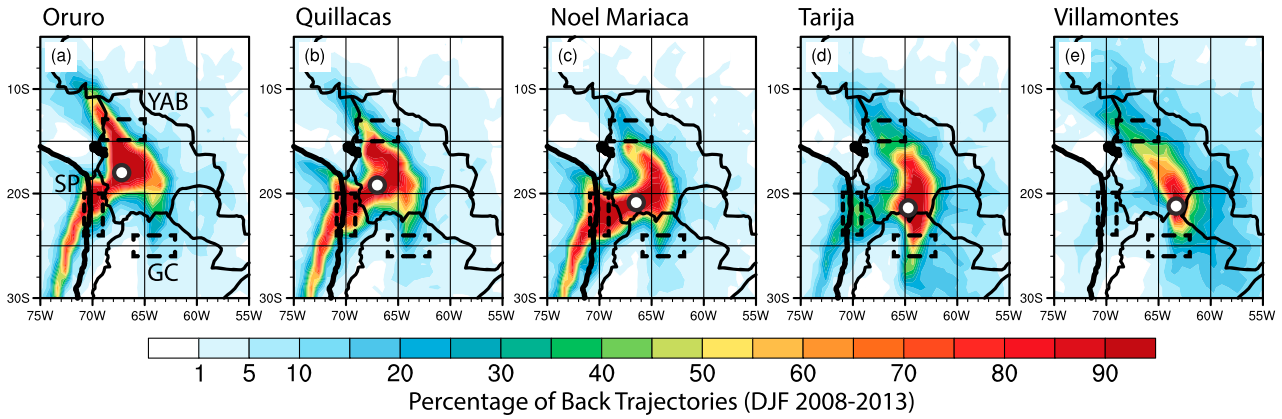

Figure 8. Composite main vapor trajectory maps for five stations in this study. We binned available trajectories to a 0.75° grid and then calculated the frequency of a trajectory passing through each grid cell. White circles denote the station location. All stations exhibit high concentrations of source trajectories along three main pathways (a): from the Yungas-Amazon Basin (YAB), the South Pacific (SP) ocean along the Chilean margin, and the Gran Chaco (GC) region, east and southeast of the Altiplano. YAB trajectory frequencies decrease from the northern to southern Altiplano (a–c). In contrast, air sourcing along the eastern flank is more diffuse but still tends to be from the YAB and GC regions (d–e).

over the Cordillera. The most likely processes to explain this pattern are continued rainout of air parcels through Rayleigh-like processes as well as vapor recycling [e.g., *Risi et al.,* 2008] and entrainment of middle and upper tropospheric vapor associated with deep convection on the Altiplano [e.g., *Moore et al.,* 2014]. Second, annual average $\delta^{18}O_p$ values for the same year can vary by ~5‰ (Figure 7a). Similarly, for single months, $\delta^{18}O_p$ values can vary by >10‰ (Figures 4a and 5a). For example, in February 2009, $\delta^{18}O_p$ values were −28.0‰ at El Choro and −15.4‰ at San Juan, and in January 2011, $\delta^{18}O_p$ values were −21.4‰ at Oruro, but −10.7‰ at Noel Mariaca. Elevation cannot account for this variability.

To better understand this variability, we calculated a correlation matrix comparing $\delta^{18}O_p$ values for each station with every other station (Table 2). Our southernmost stations on the Altiplano—Noel Mariaca and San Juan—exhibit low correlations with our other stations, while our northern Altiplano and eastern flank stations express high correlations with their neighbor stations. This pattern indicates a high likelihood that controls on southern Altiplano air sourcing and $\delta^{18}O_p$ differ from those on the northern Altiplano and the eastern flank.

Spatial patterns in $\delta^{18}O_p$ appear related to trends in air source (Figure 8). Back trajectory modeling indicates that air sources vary substantially for individual stations. Northern and central Altiplano stations (Oruro and Quillacas) show strong air sourcing from the Yungas-Amazon Basin (YAB) to the north and along a narrow pathway from the South Pacific (SP) (Figure 8). Air source regions from eastern flank stations are more diffuse, but show clear maxima in the YAB and Gran Chaco (GC) regions and significantly reduced advection from the SP. In contrast, the southern Altiplano station of Noel Mariaca shows strong air sourcing from the SP and GC regions, with a relatively reduced contribution from the YAB (Table 3, 15.3% versus 40.0% for Oruro).

Three major trends become clear from the mean partitioning between the three main air sources (Table 3). First, the northern Altiplano receives air parcels from the YAB more frequently than the southern Altiplano, consistent with prior regional climate model simulations [*Insel et al.,* 2013]. Correspondingly, the frequency of air parcels arriving from the SP and GC regions on the plateau increases from north to south. Second, the frequency of YAB-derived air parcels is higher along the eastern flank than on the southern Altiplano. This result supports the strong correlations between northern Altiplano stations and percentage of YAB parcels (Table 4). Finally, the eastern flank stations show diminished air sourcing from the SP and augmented air sourcing from the GC region compared to the plateau stations.

The proportion of trajectories from the YAB converges to ~40% for all plateau stations when we calculate air source partitioning using only trajectories that co-occur with precipitation (Table 3). The tendency of YAB trajectories to have equal importance at all Altiplano stations during precipitation events suggests that plateau $\delta^{18}O_p$ variability is related to changes in the $\delta^{18}O$ of YAB vapor and the partitioning of air between SP and GC sources. This pattern also indicates that moisture advection from the YAB is important for initiating precipitation on the southern Altiplano, but occurs less frequently overall.

Table 3. Multiyear Composite Normalized Areal Mean DJF Back Trajectory Partitioning Percentages

	Yungas-Amazon (13–15°S, 65–69°W)		South Pacific (20–24°S, 69–71°W)		Gran Chaco (24–26°S, 62–66°W)	
Station	All	Rain Only	All	Rain Only	All	Rain Only
Oruro	40.7	44.5	53.2	49.9	6.1	5.6
Quillacas	26.4	40.0	65.1	49.6	8.5	10.3
Noel Mariaca	15.3	38.3	73.5	33.2	11.2	28.5
Tarija	30.0	36.0	37.6	25.0	32.4	39.0
Villamontes	55.3	60.1	18.9	11.0	25.7	28.9

4.3. Temporal Variability of $\delta^{18}O_p$ and Air Sourcing

Our measurements of central Andes $\delta^{18}O_p$ also show significant temporal variability. Amount-weighted mean $\delta^{18}O_p$ varies from year to year for all stations, with higher interannual variability observed in the northern Altiplano and the eastern flank compared to the southern Altiplano (Figure 7). For example, annual $\delta^{18}O_p$ varied from −11.6‰ (July 2009 to June 2010) to −19.4‰ (July 2010 to June 2011) at Quillacas and −5.3‰ (August 2008 to June 09) to −9.8‰ (July 2010 to June 2011) at Tarija, but only varied from −13.1‰ (July 2009 to June 2010) to −15.8‰ (August 2008 to June 2009) at San Juan. Furthermore, the total range in annual average $\delta^{18}O_p$ observed on the plateau itself (~9‰) is approximately the same range as is observed across the entire elevation transect (Figure 7a).

High interannual variability in mean annual $\delta^{18}O_p$ could have several different causes. First, interannual variability in the large-scale circulation could result in changes in moisture source partitioning between the Atlantic and Pacific Oceans as well as the YAB or GC regions. Air masses from each of these regions are likely isotopically distinct [*Vuille et al.,* 2003a; *Sturm et al.,* 2007; *Insel et al.,* 2013], and variations in the relative balance of moisture advection in each region could alter isotopic compositions observed in the

Table 4. Correlations Between DJF Air Source Regions and Bolivian High Latitude, Monthly Precipitation Amount, and $\delta^{18}O_p$[a]

		Oruro	Quillacas	Noel Mariaca	Tarija	Villamontes
		Bolivian High Latitude				
All available trajectories	Yungas-Amazon (YAB)	0.004	−0.220	**−0.614**	**−0.808**	−0.027
	South Pacific (SP)	0.323	0.303	**0.545**	**−0.890**	−0.562
	Gran Chaco (GC)	−0.099	−0.174	0.103	0.036	0.289
Rain event trajectories only	YAB	−0.001	−0.202	**−0.574**	**−0.731**	−0.277
	SP	−0.016	0.329	0.072	**0.729**	0.383
	GC	0.030	−0.138	0.509	0.199	−0.079
		Monthly Precipitation Amount				
All available trajectories	YAB	−0.009	0.306	0.028	−0.203	−0.414
	SP	−0.057	−0.394	−0.417	0.149	−0.053
	GC	0.127	0.194	**0.538**	0.084	0.430
Rain event trajectories only	YAB	−0.030	0.176	−0.265	−0.208	−0.030
	SP	−0.120	0.107	0.319	0.515	−0.404
	GC	0.244	−0.295	0.020	−0.191	0.349
Bolivian High Latitude		0.160	−0.094	−0.139	0.221	−0.577
		Monthly $\delta^{18}O_p$				
All available trajectories	YAB	0.093	−0.051	−0.140	−0.578	−0.282
	SP	0.236	0.205	**0.547**	0.252	0.161
	GC	0.164	−0.298	**−0.563**	0.404	0.203
Rain event trajectories only	YAB	−0.056	0.135	0.052	−0.582	−0.347
	SP	−0.048	−0.129	0.213	0.186	0.366
	GC	0.149	−0.004	−0.211	0.478	−0.005
Bolivian High Latitude		**0.663**	0.409	0.079	0.463	0.560

[a]Correlation coefficients are calculated using all available trajectories, or only trajectories resulting in precipitation at the station as forecasted by the ERA-Interim reanalysis data set. Coefficients that are significant at the $p = 0.05$ level are bolded.

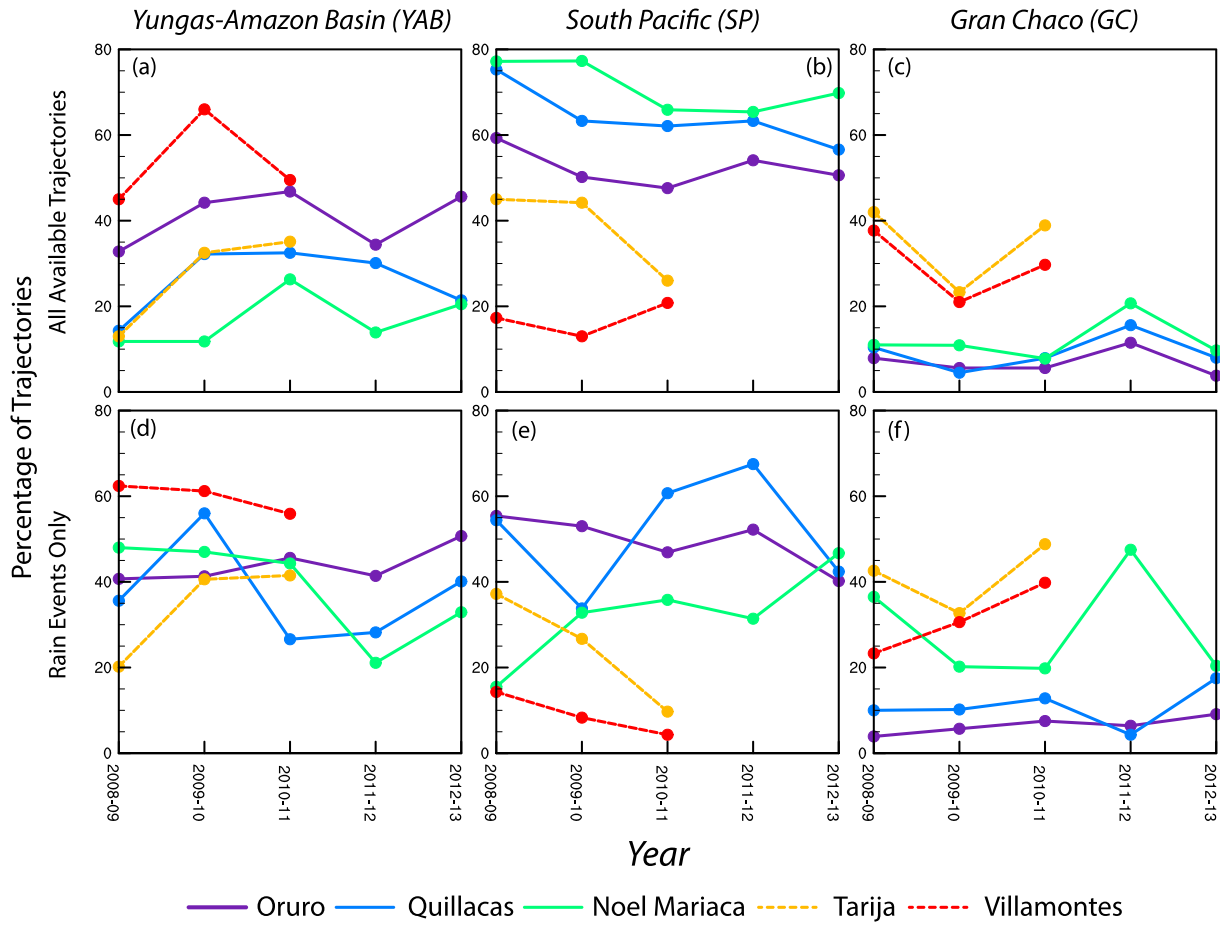

Figure 9. Rainy season trajectory frequencies from the three main source regions for five stations. (a–c) Frequency of DJF trajectories sourced from the YAB, SP, and GC regions using all trajectories. (d–f) DJF trajectory densities for only those resulting in precipitation at the station. Partitioning of air sources between stations changes on an interannual basis. Precipitation occurs most along the YAB and GC trajectories for all stations and less along the SP trajectories compared to all trajectories. We did not calculate values for Tarija and Villamontes for the 2011–2012 and 2012–2013 rainy seasons as the stations had been retired at this point.

central Andes. Alternatively, interannual variability could be related to remote precipitation processes. For example, anomalously high (low) precipitation upstream along a trajectory from the Central Andes could increase (decrease) rainout from an air parcel, and result in more (less) negative $\delta^{18}O_p$ values in the Central Andes. We investigate these two mechanisms below.

4.3.1. Changes in Large-Scale Circulation and Air Sourcing

Partitioning of air trajectories between YAB, SP, and GC pathways varies from year to year (Figure 9 and Table S10). For example, the northern Altiplano consistently receives YAB vapor more often than the eastern flank or the central and southern plateau (Figure 9a). Variability in central Andes moisture sourcing can be related to the Bolivian High, as it guides moisture transport to the central Andes through its influence on upper level winds [*Vuille et al.,* 1998; *Lenters and Cook*, 1999; *Vuille*, 1999; *Garreaud and Aceituno*, 2001; *Insel et al.,* 2013]. 200 hPa winds from ERA-Interim show that the Bolivian High position varies from season to season. During our study period, the Bolivian High reached its most northerly position during the 2011–2012 rainy season (centered at 15°S), and its most southerly position during the 2010–2011 rainy season (centered at 20°S). Positions in the other three years are all closer to the northern extreme, with maximum monthly northward (southward) excursions to 13°S (21°S) (Table S10).

Despite considerable variability in both the position of the Bolivian High and air sources, we observe few significant correlations between air sourcing and the Bolivian High. For example, we observed statistically significant ($p = 0.05$) negative correlations between the Bolivian High latitude and YAB and SP trajectory densities at Noel Mariaca ($r = -0.614$ and 0.545, respectively) and Tarija ($r = -0.808$ and 0.890) stations

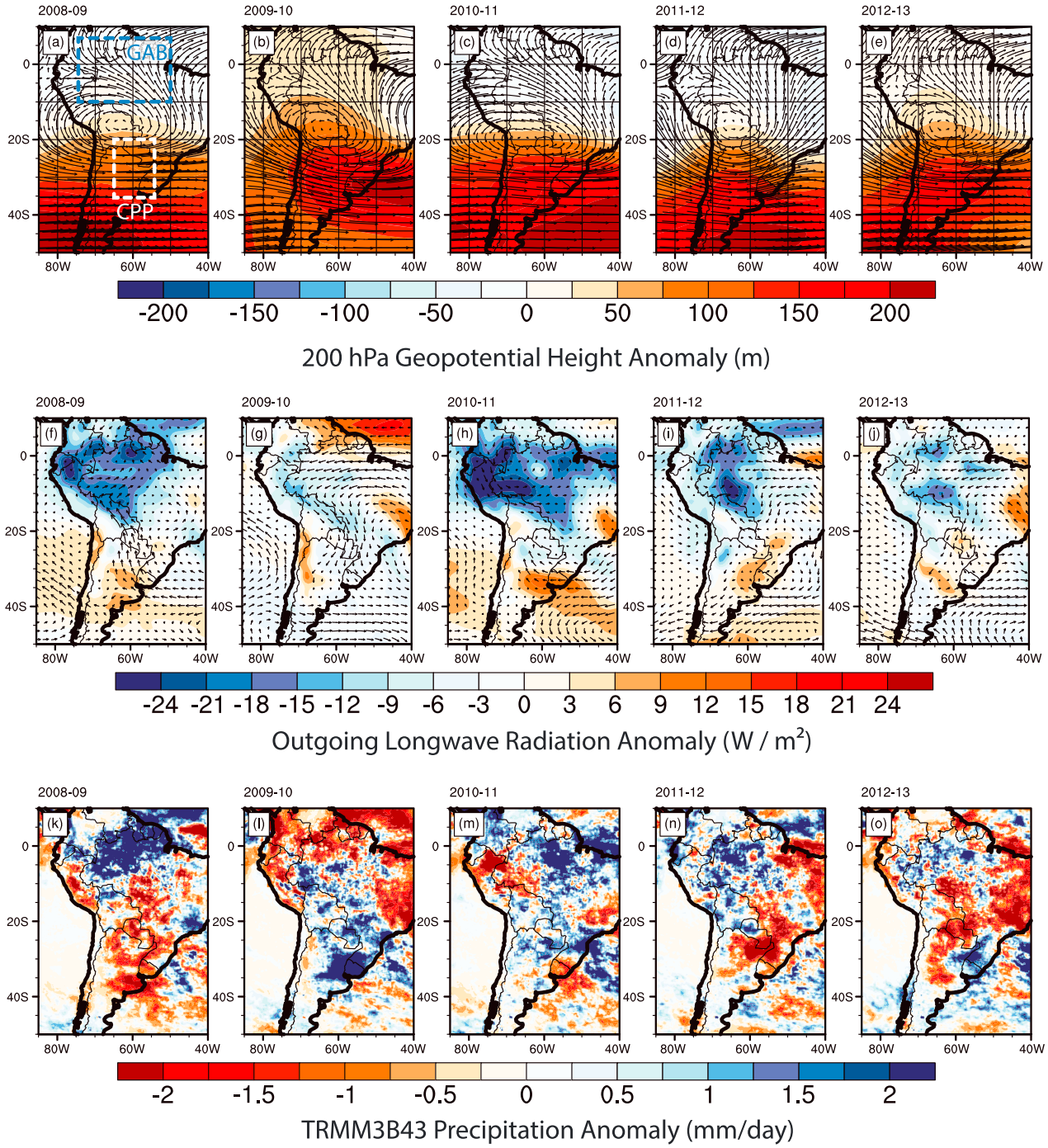

Figure 10. DJF climatic conditions relevant to central Andes $\delta^{18}O_p$ during the study period. Mean DJF 200 hPa winds (vectors, m/s) and anomalous 200 hPa geopotential height (contours, m) (a–e), anomalous DJF 850 hPa winds (vectors, m/s) and anomalous OLR (contours, W/m^2) (f–j), and anomalous DJF precipitation (k–o) for each rainy season from 2008 to 2013. Anomalies in the top two rows (Figures 10a–10j) were calculated as departure from the DJF 1979–2013 average using ERA-Interim reanalysis data and as departure from the 1998–2013 DJF average using the TRMM3B43 data set in the bottom row (Figures 10k–10o). The Greater Amazon Basin (GAB) and Chaco-Pampean Plain (CPP) are outlined in Figure 10a.

(Table 4). In contrast, we found no statistically significant relationships between the Bolivian High and GC region parcel amounts (Table 4). If we limit back trajectories to those that co-occur with station precipitation, the same patterns emerge (Table 4). In this case, however, the relationship between SP air sourcing and Bolivian High latitude at Noel Mariaca is no longer significant ($r = 0.072$).

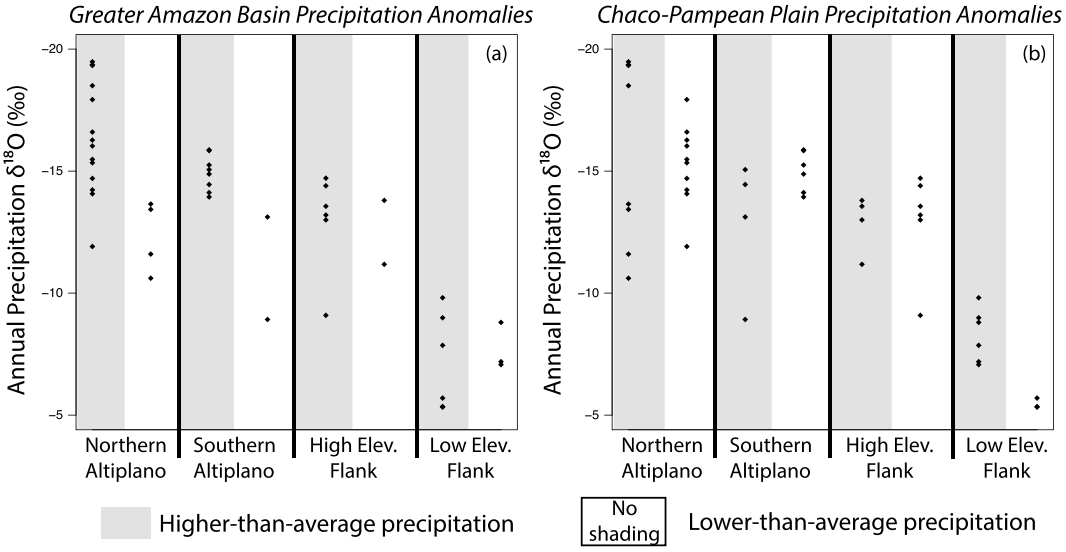

Figure 11. Strip charts showing the variability in $\delta^{18}O_p$ for the northern Altiplano (ORU, ECH, QUI, SAL), southern Altiplano (SJU, NMA), high elevation eastern flank (GCH, TUP), and low elevation eastern flank (TAR, ERI, VMO) associated with anomalies in the (a) Greater Amazon Basin (GAB) and (b) Chaco-Pampean Plain (CCP) precipitation. Periods with above average precipitation are shaded gray. Positive GAB precipitation anomalies correspond with more negative Altiplano $\delta^{18}O_p$ values. Positive CCP precipitation anomalies correspond with more negative $\delta^{18}O$ values at the low elevation stations along the plateau flank.

Linear regressions between monthly precipitation amount and monthly $\delta^{18}O_p$ values show few strong and significant ($p = 0.05$) relationships with trajectory pathway partitioning or Bolivian High latitude (Table 4). No stations have a statistically significant relationship between precipitation amount and the Bolivian High latitude; only Oruro exhibits a significant relationship between monthly $\delta^{18}O_p$ values and the Bolivian High latitude ($r = 0.663$). Similarly, no salient relationships are found between monthly $\delta^{18}O_p$ and trajectory densities. The only significant relationships between monthly $\delta^{18}O_p$ and trajectory densities (SP and GC) we found are at Noel Mariaca ($r = 0.547$ and -0.563, respectively) (Table 4). In summary, although the position of the Bolivian High influences air source pathways for parts of the central Andes, particularly for the southern plateau and portions of the eastern flank, it is not significantly correlated with either local precipitation amount or $\delta^{18}O_p$.

4.3.2. Remote Precipitation Processes

Interannual variability in precipitation amount along prominent air trajectories may result in differences in central Andean $\delta^{18}O_p$ through changes in the degree of upstream parcel rainout and vapor recycling and mixing resulting from upstream convection. Vapor sourced from regions with below average precipitation are likely to have above average (i.e., less negative) isotopic compositions, whereas vapor sourced from regions with above average precipitation are likely to have below average (i.e., more negative) isotopic compositions. To assess this possibility, we calculated areal average DJF precipitation anomalies for the Greater Amazon Basin (GAB, 7.5°N–10°S, 50–75°W) and Chaco-Pampean plain (CPP, 20–35°S, 55–65°W) (Figure 10a). These upstream regions feed vapor to the YAB and GC, respectively, and connect them to their oceanic vapor source (Figures 2a and 10a). We calculated DJF anomalies from the 1998–2013 mean for each rainy season for the GAB and CCP using the TRMM 3B43 data set [*Huffman et al.,* 2007]. SP parcels originate under a region of strong atmospheric subsidence and rarely lead to precipitation upstream of the Altiplano [*Garreaud et al.,* 2010; *Insel et al.,* 2010]; thus, we did not calculate precipitation anomalies here.

GAB and CPP precipitation amounts vary strongly from year to year. GAB precipitation was 23.0, 9.3, 9.4, and 2.3% above average during the 2008–2009, 2010–2011, 2011–2012, and 2012–2013 rainy seasons, respectively (Figures 10k and 10m–10o), and 7.8% below average during DJF 2009–2010 (Figure 10l). Positive (negative) GAB precipitation anomalies occur with more (less) negative annual average $\delta^{18}O_p$ for both the northern and southern Altiplano (Figure 11a). Stations along the eastern flank, however, show no

clear relationship between annual average $\delta^{18}O_p$ and GAB precipitation anomalies. CPP precipitation was 42.8 and 8.5% above average during the 2009–2010 and 2010–2011 rainy seasons (Figures 10l and 10m) and 22.0, 16.7, and 9.5% below average precipitation during the 2008–2009, 2011–2012, and 2012–2013 (Figures 10k, 10n, and 10o) rainy seasons. Positive (negative) precipitation anomalies in the CPP region occur with more (less) negative annual average $\delta^{18}O_p$ for low elevation eastern flank sites (<2500 m, Tarija, Entre Rios, and Villamontes). We observe no relationships between precipitation anomalies and annual average $\delta^{18}O_p$ at the high elevation eastern flank sites or on the plateau (Figure 11b). Both the GAB and CPP regions received above average precipitation during the year with the most negative $\delta^{18}O_p$ values across the northern Altiplano and eastern flank (2010–2011). No other year during our study exhibited above average precipitation for both regions. Further, the strong southerly excursion of the Bolivian High occurs with increased advection from GC and CPP regions relative to other years studied (Figures 10c and 10h; Table S10). In contrast, the year with the least negative $\delta^{18}O_p$ values across the northern Altiplano and eastern flank (2009–2010) is the only year with below average precipitation in the GAB (Figure 10l). We observe that the interannual variability is largely consistent with precipitation anomalies in major air source regions, supporting the idea that remote and upstream precipitation amount anomalies are preserved in and provide a primary control on central Andes $\delta^{18}O_p$ values and patterns. Studies investigating precipitation along the eastern Andes flank [*Vimeux et al.,* 2005, 2011], the isotopic composition of ice cores [*Grootes et al.,* 1989; *Thompson et al.,* 2013], and calcite in lake sediment cores [*Bird et al.,* 2011], have also concluded that the isotopic composition of high central Andes precipitation depends on processes in the Amazon basin.

5. Discussion

5.1. Controls on Central Andes $\delta^{18}O_p$

Elevation is the strongest regional control on $\delta^{18}O_p$ at multiyear timescales (Figures 6a and 7b). Adiabatic ascent of air masses up the eastern Andean flank promotes condensation from air parcels and subsequent and progressive removal of heavy isotopes via Rayleigh distillation, resulting in an inverse relationship between surface elevation and $\delta^{18}O_p$ [*Dansgaard*, 1964; *Siegenthaler and Oeschger*, 1980; *Rowley and Garzione*, 2007]. In addition, convective precipitation both within and upstream of the central Andes can drive measured $\delta^{18}O_p$ to lighter compositions than anticipated by Rayleigh distillation and further introduce interannual variability into $\delta^{18}O_p$ with a given increase in elevation [*Lee and Fung*, 2007; *Brown et al.,* 2008; *Risi et al.,* 2008; *Moore et al.,* 2014].

Central Andes $\delta^{18}O_p$ is highly variable in space and time (Figures 4a, 5a, and 7a). Our $\delta^{18}O_p$ time series indicate that month-to-month changes from station-to-station track each other in the northern Altiplano and along the eastern Andean flank (Table 2). Southern Altiplano $\delta^{18}O_p$ correlates poorly with eastern flank and northern Altiplano $\delta^{18}O_p$, indicating a difference in $\delta^{18}O_p$ controls. We interpret the high interannual variability observed to be principally related to precipitation anomalies upwind of the central Andes based on their close association with $\delta^{18}O_p$ anomalies (Figure 11). Increased precipitation upstream of the central Andes likely led to vapor that was more depleted in heavy isotopes through two distinct effects. First, processes related to atmospheric convection in source regions, including partial evaporation of raindrops, vapor recycling, and increased entrainment and subsequent downward mixing of isotopically lighter middle and upper troposphere vapor [*Lee and Fung*, 2007; *Risi et al.,* 2008; *Moore et al.,* 2014] all contribute to depleting low-level vapor in heavy stable isotopes. Second, increased upwind precipitation also enhances the fraction of water vapor removed from a parcel through its transport from the Atlantic Ocean to the central Andes, which would result in lighter isotopic compositions through Rayleigh distillation. We use back trajectory analysis to demonstrate that large-scale circulation in South America, namely, the position of the Bolivian High, can alter the relative importance of vapor source regions (Figures 8 and 9; Tables 3, 4, and S6). As a result, the Bolivian High modulates the influence of upstream precipitation anomalies from different regions of the continent. For example, when the Bolivian High occurs toward the northern end of its range, vapor advection decreases from the GC and CPP regions. In this way, the large-scale circulation can shield central Andean $\delta^{18}O_p$ from the influence of the strong precipitation anomalies observed in the CPP region (Figure 10g). Our $\delta^{18}O_p$ data analysis affirms prior work that notes strong associations between remote source region precipitation anomalies and eastern flank

$\delta^{18}O_p$ [e.g., *Vimeux et al.,* 2005, 2011; *Samuels-Crow et al.,* 2014a] and extends them into the plateau itself. These results are also consistent with interpretations of lake sediment and ice cores relating $\delta^{18}O$ compositions to remote precipitation intensity in the Amazon Basin [e.g., *Grootes et al.,* 1989; *Hoffmann*, 2003; *Vimeux et al.,* 2009; *Bird et al.,* 2010; 2011; *Vuille et al.,* 2012].

We cannot rule out a potentially important role for local scale controls, particularly at high temporal frequencies and small spatial scales. For example, $\delta^{18}O_p$ at two different stations at similar elevations on the Altiplano for the same month were observed to vary by up to 13‰ (Figure 4a). The magnitude of this variability is unlikely to be explained by regional-scale circulation controls and their influence on moisture sourcing. Therefore, we suggest that local variability in convective precipitation or valley-ridge scale forcing of moisture convergence and convection may also play a role in the observed variability in central Andean $\delta^{18}O_p$ values [*Giovannettone and Barros*, 2009].

Our results support the influence of the Bolivian High position in partitioning air sources for portions of the central Andes inferred from climate modeling studies [*Vuille et al.,* 1998; *Vuille and Werner*, 2005; *Insel et al.,* 2013]. For example, we observed a uniform dependence across the plateau for YAB sourced air during precipitation events (Figure 8 and Table 3). More broadly, however, we find no relationship between the Bolivian High latitude, local precipitation amount, and $\delta^{18}O_p$ (Table 4). This result calls into question links drawn from climate model results between the Bolivian High, moisture sources, precipitation amount, and central Andes $\delta^{18}O_p$ [e.g., *Vuille et al.,* 2003a; *Insel et al.,* 2013]. Our $\delta^{18}O_p$ results indicate that upstream precipitation anomalies influence $\delta^{18}O_p$ values more than the position of the Bolivian High. Additionally, multiyear amount-weighted annual mean $\delta^{18}O_p$ values derived from the REMOiso regional isotope-tracking general circulation model are heavier than observations by a few per mil at high elevations (Figure 7b) [*Insel et al.,* 2013]. We attribute these differences to the regional climate model grid, which may still be too coarse (~55 km) to resolve important topographic features and truncates the highest peaks. Despite this, the model captures the spatial patterns well. Regardless, our data set, climate model simulations, and lake sediment calcite and glacial ice $\delta^{18}O$ values highlight the importance of remote processes to central Andes $\delta^{18}O_p$. We suspect that some climate model parameterizations may be responsible for the mechanistic differences inferred. In particular, limitations in precipitation parameterization schemes used in regional climate model studies might overstate (understate) the role of local (remote) precipitation processes. Many models simulate coupling between the land surface and atmosphere that is too strong, as shown by Amazon precipitation and evapotranspiration fluxes that exceed observations by ~20% [*Insel et al.,* 2013]. Additionally, simulated precipitation amounts at the Andean flank are too large and are a result of overestimated moisture convergence in regions with steep topography [*Codron and Sadourny*, 2002; *Bala et al.,* 2008; *Insel et al.,* 2013]. Finally, assumptions made in model parameterizations of convection also influence the simulated $\delta^{18}O_p$ patterns [e.g., *Lee et al.,* 2009b]. Bias between observed and simulated $\delta^{18}O_p$ patterns and values is uncertain and likely model dependent because different models often employ different convection schemes. Despite these uncertainties, climate model simulations remain valuable tools to understand the dynamic processes influencing $\delta^{18}O_p$.

5.2. ENSO and Central Andes $\delta^{18}O_p$

ENSO introduces significant interannual variability into South American climate patterns [*Garreaud et al.,* 2009]. This variability likely influences central Andes $\delta^{18}O_p$ values. ENSO variability significantly impacts precipitation amount and large-scale circulation on the Altiplano as well as in the main source regions such as the Amazon Basin and southeastern South America [*Garreaud and Battisti*, 1999; *Vuille et al.,* 2000; *Garreaud et al.,* 2009]. In general, ENSO is associated with strong precipitation anomalies in different regions and results in more (less) negative $\delta^{18}O_p$ values when source regions experience enhanced (suppressed) rainout [*Garreaud et al.,* 2009; *Insel et al.,* 2013]. ENSO variability has also been observed in central Andes ice cores [*Henderson et al.,* 1999; *Bradley et al.,* 2003; *Vimeux et al.,* 2009].

Several ENSO events occurred during the study period: a relatively strong El Niño occurred during winter 2009–2010, while a relatively strong La Niña occurred during 2010–2011 and weak La Niña conditions were observed during 2008–2009 and 2011–2012 [after *Smith et al.,* 2008; *National Centers for Environmental Prediction*, 2014]. On the Altiplano, El Niño (La Niña) conditions are frequently associated with decreased (increased) moisture advection from the east by strengthened (weakened) westerly middle and upper level

winds [*Vuille*, 1999; *Vuille et al.,* 2000; *Garreaud and Aceituno*, 2001]. This trend is consistent with observed shifts in the position of the Bolivian High during the study period during the strongest ENSO events. During the 2010/2011 La Niña, the Bolivian High was at its southernmost position during the study (Figure 10c), promoting abnormally strong easterly winds over the Altiplano and facilitating moisture convergence from both the GAB and CPP regions and driving $\delta^{18}O_p$ to more negative values. In contrast, during the 2009/2010 El Niño, the Bolivian High was positioned further northward and abnormally strong (Figure 10b), enhancing upper level westerly winds and inhibiting moisture convergence, suppressing parcel rainout, and causing less negative $\delta^{18}O_p$ values.

ENSO influences the GAB in the same manner as it influences the Altiplano. El Niño (La Niña) events are associated with decreased (increased) DJF precipitation in the GAB. This pattern occurs with increased (decreased) continental subsidence coincident with increased (decreased) convection off the western coast of South America [*Marengo*, 1992; *Liebmann and Marengo*, 2001]. Together, this pattern facilitates decreased (increased) parcel rainout and less (more) negative $\delta^{18}O_p$ values. This pattern is observed during this study, with positive precipitation anomalies observed in all La Niña years and strong negative precipitation anomalies observed during the lone El Niño year. ENSO also similarly affects precipitation amounts along the eastern margin, potentially through changes in the SALLJ [*Ronchail et al.,* 2005; *Ronchail and Gallaire*, 2006]. In contrast, ENSO manifests in the opposite pattern in the CPP compared to the Altiplano or GAB, as a result of changes in the midlatitude jet [*Barros and Silvestri*, 2002; *Silvestri*, 2004]. This pattern is generally observed in our study except during the 2010–2011 rainy season, when precipitation in the CPP is above average despite a strong La Niña, further facilitating more negative central Andean $\delta^{18}O_p$. Our results indicate that the relationship between central Andes $\delta^{18}O_p$ and ENSO is complex, as previously suggested in interpretations of regional ice cores [e.g., *Henderson et al.,* 1999; *Vimeux et al.,* 2009].

5.3. Implications for Paleoclimate and Paleoaltimetry

The isotopic composition of precipitation is preserved in proxy materials that trap or form from precipitation (e.g., ice cores and hydrated volcanic glass) or form in equilibrium with precipitation (e.g., pedogenic carbonates and authigenic clays). In the central Andes and South America as a whole, these proxies have been used to constrain and understand changes in paleohydrology [e.g., *Baker et al.,* 2001; *Wang et al.,* 2004; *Ekdahl et al.,* 2008], paleoclimate [e.g., *Thompson et al.,* 1998; *Vimeux et al.,* 2009; *Mulch et al.,* 2010], and paleoelevation [e.g., *Garzione et al.,* 2008; *Leier et al.,* 2013; *Saylor and Horton*, 2014]. A challenge for interpreting these proxy records is that the modern distribution and spatial variability of modern water isotopologues have historically been poorly known, particularly across the Altiplano. Moreover, the data demonstrate a high degree of interannual and spatial variability in the region, an understanding of which is required for informed interpretations of the paleoclimate and paleoaltimetric proxy record [e.g., *Vuille et al.,* 2003a; *Lee et al.,* 2009a; *Lewis et al.,* 2010; *Insel et al.,* 2012]. High variability is also observed in modern Nevado Sajama snow $\delta^{18}O$ [*Hardy et al.,* 2003], indicating that this variability can also be reflected in materials such as ice that preserve a $\delta^{18}O$ sequence. This high interannual variability collectively indicates that modern observational records with short time spans may be biased toward climatic extremes. For example, data from the Yungas-Altiplano transect in *Gonfiantini et al.* [2001] spans the 1983 El Niño and the 1984 La Niña. Thus, none of the modern precipitation data prior to this study actually constrain $\delta^{18}O_p$ patterns during a neutral ENSO phase. Therefore, modern isotopologue distributions can be biased and hence be poor representations of the past. This reality may impact how robust interpretations of proxy compositions are when they are compared to possibly poorly representative modern values.

The impact of this modern observational bias will vary depending on the length of time represented by the proxy. The frequency of climate variability resolved by proxies varies by proxy type and age and ranges from subannual to several millennia. Ice and lake sediment cores record subannual to decadal variability [*Thompson et al.,* 1984; *Bird et al.,* 2010, 2011; *Thompson et al.,* 2013], while pedogenic carbonates and hydrated volcanic glass acquire their isotopic composition over thousands of years [*Cerling and Quade*, 1993; *Friedman et al.,* 1993; *Mulch and Chamberlain*, 2007; *Quade et al.,* 2007]. As a result of the wide range of timescales encapsulated by proxy materials, we suggest that our results have greater implications for proxies with longer integration periods for two primary reasons. First, as ice cores and lake cores resolve

subannual to decadal variability, the large range of (near) modern isotopic compositions is well known [*Hardy et al.,* 2003], as is its relationship to tropical climate variability [e.g., *Bradley et al.,* 2003; *Bird et al.,* 2010]. Second, for proxies that form over longer periods (century to millennia), it remains less clear whether the compositions preserved in pedogenic carbonates or hydrated volcanic glass represent long-term mean annual conditions, seasonal conditions, or even extreme conditions [e.g., *Cerling and Quade*, 1993; *Breecker et al.,* 2009; *Peters et al.,* 2013]. Our extended (~5 years) isotopic record presented here can be used to better evaluate the fidelity with which various proxies represent the environments under which they form.

Finally, controls on central Andean $\delta^{18}O_p$ vary spatially, and therefore, proxies from different regions may not record equivalent processes nor be directly comparable due to the strong north-south gradients we observed. It is also likely these gradients were not constant throughout the Cenozoic due to the strong alteration of South American climate induced by the rise of the Andes [e.g., *Ehlers and Poulsen*, 2009; *Insel et al.,* 2010; *Mulch et al.,* 2010; *Poulsen et al.,* 2010; *Barnes et al.,* 2012]. Furthermore, Andean uplift may have contributed to the evolution of modern ENSO dynamics [*Feng and Poulsen*, 2014]. Thus, the strong influence of atmospheric circulation on central Andes $\delta^{18}O_p$ compels future paleometeoric water isotopologue studies to carefully consider that coevolving changes in atmospheric circulation, climate, and topography combine to influence these proxy records in ways that remain difficult to simplify and disentangle. Despite uncertainties and limitations, further (paleo)climate model simulations and field-based observations offer a multipronged approach for disentangling these coupled processes and addressing proxy interpretation ambiguities.

6. Conclusions

We address key gaps and uncertainties in our observations and understanding of $\delta^{18}O_p$ patterns in modern central Andes rainfall. Elevation provides the dominant control across multiyear timescales. However, the $\delta^{18}O_p$-elevation relationship varies in space and time and does not adequately predict $\delta^{18}O_p$ across the Bolivian Altiplano. We also show that observed interannual variability in $\delta^{18}O_p$ is directly related to South American synoptic circulation. First, we confirm anomalous precipitation amounts in upwind air source regions control both Altiplano and eastern flank $\delta^{18}O_p$. The most likely explanation is changes in the fraction of water vapor removed from an air parcel upwind, which influences Altiplano $\delta^{18}O_p$ via convective processes and Rayleigh fractionation associated with parcel rainout [*Vimeux et al.,* 2005; *Vuille and Werner*, 2005; *Samuels-Crow et al.,* 2014a]. Second, we show that the Bolivian High modulates the influence of the Amazon and Gran Chaco air source regions and thus their potential effect on central Andes $\delta^{18}O_p$. These controls are consistent with prior studies along other parts of the Eastern Cordillera in the Andes [*Vimeux et al.,* 2005, 2011], but we extend them to the central plateau. Further, our results support insights from isotope-tracking climate models that central Andes $\delta^{18}O_p$ patterns respond to continental-scale climate variability [e.g., *Vuille et al.,* 2003a; *Vuille and Werner*, 2005; *Insel et al.,* 2013]. However, our results suggest that models overestimate the direct role of large-scale circulation and underestimate the role of anomalous upwind precipitation, which we attribute to shortcomings in the model parameterization of precipitation. On short timescales (1 month to $<$ 1 year), we find variability on small spatial scales (~50 km) that cannot be explained by elevation nor regional-scale circulation patterns. We speculate that local variability in precipitation amount and convection intensity further depletes heavy isotopes in precipitation leading to more negative $\delta^{18}O_p$ values than would be otherwise expected. Finally, we find high interannual variability (approaching 50% of the mean) in the average isotopic lapse rate often used in paleoelevation reconstructions [e.g., *Rowley and Garzione*, 2007], which is consistent with isotope-tracking climate model results [*Insel et al.,* 2013]. Prior and limited observations of modern central Andes $\delta^{18}O_p$ coincided with ENSO extremes and thus have likely been biased by such climatic extremes and hence may not be representative over geologic timescales. Our longer data set better constrains the role of climate variability on central Andes $\delta^{18}O_p$ and elucidates a close link with South American circulation. Therefore, we recommend that future paleoclimate and paleoaltimetric studies based on $\delta^{18}O_p$ require both an (a) understanding of paleocirculation dynamics and (b) improved acknowledgement, perhaps by incorporating more conservative uncertainty estimates, for the natural variability in $\delta^{18}O_p$-elevation relationships across space and time.

Acknowledgments

Monthly isotope and micrometeorological are available in the supporting information. Other data sources used in this analysis are freely available for academic use: TRMM data are available from the NASA Mirador portal (http://mirador.gsfc.nasa.gov), ERA-Interim is available from the ECMWF data portal (http://apps.ecmwf.int/datasets/data/interim_full_mnth/), DEM data used in this study are available from the WWF HydroSHEDS project (http://hydrosheds.cr.usgs.gov/index.php), and the University of Delaware Climate Dataset is available for download at the Department of Geography Center for Climatic Research website (http://climate.geog.udel.edu/~climate/). GNIP isotopic data are available from the IAEA-Water Resources Program (http://www-naweb.iaea.org/napc/ih/IHS_resources_gnip.html). We acknowledge several funding sources for this work: RPF received an NSF Graduate Research Fellowship (grant 2011094378), a University of Michigan Graduate Student Research Grant, a University of Michigan Rackham Graduate School International Research Award, and two University of Michigan Department of Earth and Environmental Sciences Scott Turner Awards. C.J.P. and T.A.E. received support from NSF EAR grants 0738822 and 0907817. C.J.P. also received support through the University of Michigan Associate Professor Fund. We thank J. Tito, G. Gonzalez, and S. Tawackoli for field logistics and support; M.L. Jeffery, N. Insel, and M. Tracy for assistance in the field; and N. Insel for access to REMOiso model data.

References

Aceituno, P. (1988), On the functioning of the Southern Oscillation in the South American sector. Part I: Surface climate, *Mon. Weather Rev.*, *116*(3), 505–524.

Aggarwal, P. K., O. A. Alduchov, K. O. Froehlich, L. J. Araguas-Araguas, N. C. Sturchio, and N. Kurita (2012), Stable isotopes in global precipitation: A unified interpretation based on atmospheric moisture residence time, *Geophys. Res. Lett.*, *39*, L11705, doi:10.1029/2012GL051937.

Aravena, R., O. Suzuki, H. Pena, A. Pollastri, H. Fuenzalida, and A. Grilli (1999), Isotopic composition and origin of the precipitation in Northern Chile, *Appl. Geochem.*, *14*, 411–422, doi:10.1016/S0883-2927(98)00067-5.

Baker, P., C. Rigsby, G. Seltzer, S. Fritz, T. Lowenstein, N. Bacher, and C. Veliz (2001), Tropical climate changes at millennial and orbital timescales on the Bolivian Altiplano, *Nature*, *409*(6821), 698–701.

Bala, G., R. B. Rood, D. Bader, A. Mirin, D. Ivanova, and C. Drui (2008), Simulated climate near steep topography: Sensitivity to methods for atmospheric transport, *Geophys. Res. Lett.*, *35*, L14807, doi:10.1029/2008GL033204.

Barnes, J. B., and T. A. Ehlers (2009), End member models for Andean Plateau uplift, *Earth Sci. Rev.*, *97*(1–4), 105–132, doi:10.1016/j.earscirev.2009.08.003.

Barnes, J. B., T. A. Ehlers, N. Insel, N. McQuarrie, and C. J. Poulsen (2012), Linking orography, climate, and exhumation across the central Andes, *Geology*, *40*(12), 1135–1138, doi:10.1130/G33229.1.

Barros, V. R., and G. E. Silvestri (2002), The relation between sea surface temperature at the subtropical south-central Pacific and precipitation in southeastern South America, *J. Clim.*, *15*(3), 251–267.

Bershaw, J., C. N. Garzione, P. Higgins, B. J. MacFadden, F. Anaya, and H. Alvarenga (2010), Spatial-temporal changes in Andean plateau climate and elevation from stable isotopes of mammal teeth, *Earth Planet. Sci. Lett.*, *289*(3–4), 530–538, doi:10.1016/j.epsl.2009.11.047.

Bershaw, J., S. M. Penny, and C. N. Garzione (2012), Stable isotopes of modern water across the Himalaya and eastern Tibetan Plateau: Implications for estimates of paleoelevation and paleoclimate, *J. Geophys. Res.*, *117*, D02110, doi:10.1029/2011JD016132.

Bird, B. W., M. B. Abbott, D. T. Rodbell, and M. Vuille (2010), Holocene tropical South American hydroclimate revealed from a decadally resolved lake sediment δ^{18}O record, *Earth Planet. Sci. Lett.*, *310*(3–4), 192–202, doi:10.1016/j.epsl.2011.08.040.f.

Bird, B. W., M. B. Abbott, M. Vuille, D. T. Rodbell, N. D. Stansell, and M. F. Rosenmeier (2011), A 2,300-year-long annually resolved record of the South American summer monsoon from the Peruvian Andes, *Proc. Natl. Acad. Sci. U.S.A.*, *108*(21), 8583–8588, doi:10.1073/pnas.1003719108.

Blisniuk, P. M., and L. Stern (2005), Stable isotope paleoaltimetry: A critical review, *Am. J. Sci.*, *305*(10), 1033–1074, doi:10.2475/ajs.305.10.1033.

Blossey, P. N., Z. Kuang, and D. M. Romps (2010), Isotopic composition of water in the tropical tropopause layer in cloud-resolving simulations of an idealized tropical circulation, *J. Geophys. Res.*, *115*, D24309, doi:10.1029/2010JD014554.

Bony, S., C. Risi, and F. Vimeux (2008), Influence of convective processes on the isotopic composition (δ^{18}O and δD) of precipitation and water vapor in the tropics: 1. Radiative-convective equilibrium and Tropical Ocean–Global Atmosphere–Coupled Ocean–atmosphere Response Experiment (TOGA-COARE) simulations, *J. Geophys. Res.*, *113*, D19305, doi:10.1029/2008JD009942.

Bowen, G. J., and J. Revenaugh (2003), Interpolating the isotopic composition of modern meteoric precipitation, *Water. Resour. Res.*, *39*(10), 1299, doi:10.1029/2003WR002086.

Bowen, G. J., and B. H. Wilkinson (2002), Spatial distribution of δ^{18}O in meteoric precipitation, *Geology*, *30*(4), 315–318.

Bradley, R. S., M. Vuille, and D. R. Hardy (2003), Low latitude ice cores record Pacific sea surface temperatures, *Geophys. Res. Lett.*, *30*(4), 1174, doi:10.1029/2002GL016546.

Breecker, D. O., Z. D. Sharp, and L. D. McFadden (2009), Seasonal bias in the formation and stable isotopic composition of pedogenic carbonate in modern soils from central New Mexico, USA, *Geol. Soc. Am. Bull.*, *121*(3–4), 630–640, doi:10.1130/B26413.1.

Brown, D. P., J. Worden, and D. C. Noone (2008), Comparison of atmospheric hydrology over convective continental regions using water vapor isotope measurements from space, *J. Geophys. Res.*, *113*, D15124, doi:10.1029/2007JD009676.

Burnham, K. P., and D. R. Anderson (2002), *Model Selection and Multimodel Inference: A Practical Information-Theoretic Approach*, 2nd ed., Springer, Heidelberg, Germany.

Campetella, C. M., and C. S. Vera (2002), The influence of the Andes mountains on the South American low-level flow, *Geophys. Res. Lett.*, *29*(17), 1826, doi:10.1029/2002GL015451.

Cerling, T. E., and J. Quade (1993), Stable carbon and oxygen isotopes in soil carbonates, in *Climate Change in Continental Isotopic Records*, vol. 78, edited by P. K. Swart et al., pp. 217–231, AGU, Washington, D. C.

Codron, F., and R. Sadourny (2002), Saturation limiters for water vapour advection schemes: Impact on orographic precipitation, *Tellus A*, *54*(4), 338–349.

Craig, H. (1961), Isotopic variations in meteoric waters, *Science*, *133*(3465), 1702.

Craig, H., and L. I. Gordon (1965), Deuterium and oxygen-18 variations in the ocean and the marine atmosphere, in *Stable Isotopes in Oceanographic Studies and Paleotemperatures*, edited by E. Tongiorgi, pp. 9–130, Laboratorio Di Geologia Nucleare, Pisa, Italy.

Dansgaard, W. (1964), Stable isotopes in precipitation, *Tellus*, *16*(4), 436–468.

Dee, D. P., et al. (2011), The ERA-Interim reanalysis: Configuration and performance of the data assimilation system, *Q. J. R. Meteorol. Soc.*, *137*(656), 553–597, doi:10.1002/qj.828.

Dessler, A. E., and S. C. Sherwood (2003), A model of HDO in the tropical tropopause layer, *Atmos. Chem. Phys.*, *3*(6), 2173–2181.

Draxler, R. R., and G. D. Hess (1998), An overview of the HYSPLIT_4 modelling system for trajectories, dispersion and deposition, *Aust. Meteorol. Mag.*, *47*(4), 295–308.

Ehlers, T. A., and C. J. Poulsen (2009), Influence of Andean uplift on climate and paleoaltimetry estimates, *Earth Planet. Sci. Lett.*, *281*(3–4), 238–248, doi:10.1016/j.epsl.2009.02.026.

Ekdahl, E., S. Fritz, P. Baker, C. Rigsby, and K. Coley (2008), Holocene multidecadal-to millennial-scale hydrologic variability on the South American Altiplano, *Holocene*, *18*(6), 867.

Feng, R., and C. J. Poulsen (2014), Andean elevation control on tropical Pacific climate and ENSO, *Paleoceanography*, *29*, 795–809, doi:10.1002/2014PA002640.

Friedman, I., G. I. Smith, J. D. Gleason, A. Warden, and J. M. Harris (1992), Stable isotope composition of waters in southeastern California. 1. Modern precipitation, *J. Geophys. Res.*, *97*(D5), 5795–5812, doi:10.1029/92JD00184.

Friedman, I., J. Gleason, and A. Warden (1993), Ancient climate from deuterium content of water in volcanic glass, in *Climate Change Continental Isotopic Records*, vol. 78, edited by P. K. Swart et al., pp. 309–319, AGU, Washington, D. C.

Garreaud, R. D., and P. Aceituno (2001), Interannual rainfall variability over the South American Altiplano, *J. Clim.*, *14*(12), 2779–2789.

Garreaud, R. D., and D. S. Battisti (1999), Interannual (ENSO) and interdecadal (ENSO-like) variability in the Southern Hemisphere tropospheric circulation*, *J. Clim.*, *12*(7), 2113–2123.

Garreaud, R. D., M. Vuille, and A. Clement (2003), The climate of the Altiplano: Observed current conditions and mechanisms of past changes, *Palaeogeogr. Palaeoclimatol. Palaeoecol.*, *194*(1–3), 5–22.
Garreaud, R. D., M. Vuille, R. Compagnucci, and J. A. Marengo (2009), Present-day South American climate, *Palaeogeogr. Palaeoclimatol. Palaeoecol.*, *281*(3–4), 180–195, doi:10.1016/j.palaeo.2007.10.032.
Garreaud, R. D., A. Molina, and M. Farias (2010), Andean uplift, ocean cooling and Atacama hyperaridity: A climate modeling perspective, *Earth Planet. Sci Lett.*, *292*(1–2), 39–50, doi:10.1016/j.epsl.2010.01.017.
Garzione, C. N., G. D. Hoke, J. C. Libarkin, S. Withers, B. J. MacFadden, J. M. Eiler, P. Ghosh, and A. Mulch (2008), Rise of the Andes, *Science*, *320*(5881), 1304–1307, doi:10.1126/science.1148615.
Gat, J. R. (1996), Oxygen and hydrogen isotopes in the hydrologic cycle, *Annu. Rev. Earth Planet. Sci.*, *24*(1), 225–262, doi:10.1146/annurev.earth.24.1.225.
Giovannettone, J. P., and A. P. Barros (2009), Probing regional orographic controls of precipitation and cloudiness in the central Andes using satellite data, *J. Hydrometeorol.*, *10*(1), 167–182, doi:10.1175/2008JHM973.1.
Giovanni, M. K., B. K. Horton, C. N. Garzione, B. McNulty, and M. Grove (2010), Extensional basin evolution in the Cordillera Blanca, Peru: Stratigraphic and isotopic records of detachment faulting and orogenic collapse in the Andean hinterland, *Tectonics*, *29*, TC6007, doi:10.1029/2010TC002666.
Gonfiantini, R., M. A. Roche, J. C. Olivry, J. C. Fontes, and G. M. Zuppi (2001), The altitude effect on the isotopic composition of tropical rains, *Chem. Geol.*, *181*(1), 147–167.
Grell, G. A. (1993), Prognostic evaluation of assumptions used by cumulus parameterizations, *Mon. Weather Rev.*, *121*(3), 764–787.
Grootes, P. M., M. Stuiver, L. G. Thompson, and E. Mosley-Thompson (1989), Oxygen isotope changes in tropical ice, Quelccaya, Peru, *J. Geophys. Res.*, *94*(D1), 1187–1194, doi:10.1029/JD094iD01p01187.
Hardy, D. R., M. Vuille, and R. S. Bradley (2003), Variability of snow accumulation and isotopic composition on Nevado Sajama, Bolivia, *J. Geophys. Res.*, *108*(D22), 4693–4702, doi:10.1029/2003JD003623.
Henderson, K. A., L. G. Thompson, and P.-N. Lin (1999), Recording of El Niño in ice core δ^{18}O records from Nevado Huascarán, Peru, *J. Geophys. Res.*, *104*(D24), 31,053–31,065, doi:10.1029/1999JD900966.
Hoffmann, G. (2003), Coherent isotope history of Andean ice cores over the last century, *Geophys. Res. Lett.*, *30*(4), 1–4, doi:10.1029/2002GL014870.
Hoke, G. D., C. N. Garzione, D. Araneo, C. Latorre, M. R. Strecker, and K. Williams (2009), The stable isotope altimeter: Do Quaternary pedogenic carbonates predict modern elevations?, *Geology*, *37*(11), 1015–1018.
Horita, J., and D. J. Wesolowski (1994), Liquid–vapor fractionation of oxygen and hydrogen isotopes of water from the freezing to the critical temperature, *Geochim. Cosmochim. Acta*, *58*(16), 3425–3437.
Huffman, G. J. (1997), Estimates of root-mean-square random error for finite samples of estimated precipitation, *J. Appl. Meteorol.*, *36*(9), 1191–1201.
Huffman, G. J., D. T. Bolvin, E. J. Nelkin, D. B. Wolff, R. F. Adler, G. Gu, Y. Hong, K. P. Bowman, and E. F. Stocker (2007), The TRMM Multisatellite Precipitation Analysis (TMPA): Quasi-global, multiyear, combined-sensor precipitation estimates at fine scales, *J. Hydrometeorol.*, *8*(1), 38–55, doi:10.1175/JHM560.1.
Iguchi, T., T. Kozu, J. Kwiatkowski, R. Meneghini, J. Awaka, and K. Okamoto (2009), Uncertainties in the rain profiling algorithm for the TRMM precipitation radar, *J. Meteorol. Soc. Jpn.*, *87A*, 1–30, doi:10.2151/jmsj.87A.1.
Insel, N., C. J. Poulsen, and T. A. Ehlers (2010), Influence of the Andes Mountains on South American moisture transport, convection, and precipitation, *Clim. Dyn.*, *35*(7–8), 1477–1492, doi:10.1007/s00382-009-0637-1.
Insel, N., C. J. Poulsen, T. A. Ehlers, and C. Sturm (2012), Response of meteoric δ^{18}O to surface uplift—Implications for Cenozoic Andean Plateau growth, *Earth Planet. Sc. Lett.*, *317–318*, 262–272, doi:10.1016/j.epsl.2011.11.039.
Insel, N., C. J. Poulsen, C. Sturm, and T. A. Ehlers (2013), Climate controls on Andean precipitation δ^{18}O interannual variability, *J. Geophys. Res. Atmos.*, *118*, 9721–9742, doi:10.1002/jgrd.50619.
Jeffery, M. L., C. J. Poulsen, and T. A. Ehlers (2012), Impacts of Cenozoic global cooling, surface uplift, and an inland seaway on South American paleoclimate and precipitation δ^{18}O, *Geol. Soc. Am. Bull.*, *124*(3–4), 335–351, doi:10.1130/B30480.1.
Kousky, V. E. (1988), Pentad outgoing longwave radiation climatology for the South American sector, *Rev. Bras. Meteorol.*, *3*(1), 217–231.
Kuang, Z., G. Toon, P. O. Wennberg, and Y. L. Yung (2003), Measured HDO/H2O ratios across the tropical tropopause, *Geophys. Res. Lett.*, *30*(7), 1372, doi:10.1029/2003GL017023.
Lechler, A. R., and J. Galewsky (2013), Refining paleoaltimetry reconstructions of the Sierra Nevada, California, using air parcel trajectories, *Geology*, *41*(2), 259–262, doi:10.1130/G33553.1.
Lechler, A. R., and N. A. Niemi (2012), Controls on the Spatial Variability of Modern Meteoric ^{18}O: Empirical Constraints from the Western U.S. and East Asia and Implications for Stable Isotope Studies, *Am. J. Sci.*, *311*(8), 664–700, doi:10.2475/08.2011.02.
Lee, J.-E., and I. Fung (2007), "Amount effect" of water isotopes and quantitative analysis of post-condensation processes, *Hydrol. Processes*, *22*(1), 1–8, doi:10.1002/hyp.6637.
Lee, J.-E., K. Johnson, and I. Fung (2009a), Precipitation over South America during the Last Glacial Maximum: An analysis of the "amount effect" with a water isotope-enabled general circulation model, *Geophys. Res. Lett.*, *36*, L19701, doi:10.1029/2009GL039265.
Lee, J.-E., R. T. Pierrehumbert, A. Swann, and B. R. Lintner (2009b), Sensitivity of stable water isotopic values to convective parameterization schemes, *Geophys. Res. Lett.*, *36*, L23801, doi:10.1029/2009GL040880.
Legates, D. R., and C. J. Willmott (1990a), Mean seasonal and spatial variability in gauge-corrected, global precipitation, *Int. J. Climatol.*, *10*(2), 111–127.
Legates, D. R., and C. J. Willmott (1990b), Mean seasonal and spatial variability in global surface air-temperature, *Theor. Appl. Climatol.*, *41*(1–2), 11–21.
Lehner, B., K. Verdin, and A. Jarvis (2008), New global hydrography derived from spaceborne elevation data, *Eos Trans. AGU*, *89*(10), 93, doi:10.1029/2008EO100001.
Leier, A., N. McQuarrie, C. Garzione, and J. Eiler (2013), Stable isotope evidence for multiple pulses of rapid surface uplift in the Central Andes, Bolivia, *Earth Planet. Sci Lett.*, *371–372*(C), 49–58, doi:10.1016/j.epsl.2013.04.025.
Lenters, J., and K. Cook (1999), Summertime precipitation variability over South America: Role of the large-scale circulation, *Mon. Weather Rev.*, *127*(3), 409–431.
Lewis, S. C., A. N. LeGrande, M. Kelley, and G. A. Schmidt (2010), Water vapour source impacts on oxygen isotope variability in tropical precipitation during Heinrich events, *Clim. Past*, *6*(3), 325–343, doi:10.5194/cp-6-325-2010.
Liebmann, B., and J. Marengo (2001), Interannual variability of the rainy season and rainfall in the Brazilian Amazon Basin, *J. Clim.*, *14*(22), 4308–4318.

Liu, Z., G. J. Bowen, and J. M. Welker (2010), Atmospheric circulation is reflected in precipitation isotope gradients over the conterminous United States, *J. Geophys. Res.*, *115*, D22120, doi:10.1029/2010JD014175.
Liu, Z., D. Ostrenga, W. Teng, and S. Kempler (2012), Tropical Rainfall Measuring Mission (TRMM) precipitation data and services for research and applications, *Bull. Am. Meteorol. Soc.*, *93*(9), 1317–1325, doi:10.1175/BAMS-D-11-00152.1.
Majoube, M. (1971), Fractionnement en oxygene-18 et en deuterium entre l'eau et sa vapeur, *J. Chem. Phys. Phys.Chim. Biol.*, *68*(10), 1423–1436.
Marengo, J. A. (1992), Interannual variability of surface climate in the Amazon basin, *Int. J. Climatol.*, *12*(8), 853–863.
Moore, M., Z. Kuang, and P. N. Blossey (2014), A moisture budget perspective of the amount effect, *Geophys. Res. Lett.*, *41*, 1329–1335, doi:10.1002/2013GL058302.
Mulch, A., and C. P. Chamberlain (2007), Stable isotope paleoaltimetry in orogenic belts — The silicate record in surface and crustal geological archives, *Rev. Mineral. Geochem.*, *66*(1), 89–118, doi:10.2138/rmg.2007.66.4.
Mulch, A., C. E. Uba, M. R. Strecker, R. Schoenberg, and C. P. Chamberlain (2010), Late Miocene climate variability and surface elevation in the central Andes, *Earth Planet. Sci. Lett.*, *290*(1–2), 173–182, doi:10.1016/j.epsl.2009.12.019.
National Centers for Environmental Prediction (2014), NCEP Oceanic Niño Index. [Available at http://www.cpc.ncep.noaa.gov/products/analysis_monitoring/ensostuff/ensoyears.shtml, Accessed 12 November 2014.]
Noone, D. C. (2012), Pairing measurements of the water vapor isotope ratio with humidity to deduce atmospheric moistening and dehydration in the tropical midtroposphere, *J. Clim.*, *25*(13), 4476–4494, doi:10.1175/JCLI-D-11-00582.1.
Peters, N. A., K. W. Huntington, and G. D. Hoke (2013), Hot or not? Impact of seasonally variable soil carbonate formation on paleotemperature and O-isotope records from clumped isotope thermometry, *Earth Planet. Sci. Lett.*, *361*, 208–218, doi:10.1016/j.epsl.2012.10.024.
Poulsen, C. J., and M. L. Jeffery (2011), Climate change imprinting on stable isotopic compositions of high-elevation meteoric water cloaks past surface elevations of major orogens, *Geology*, doi:10.1130/G32052.1.
Poulsen, C. J., T. A. Ehlers, and N. Insel (2010), Onset of convective rainfall during gradual Late Miocene rise of the central Andes, *Science*, *328*(5977), 490–493, doi:10.1126/science.1185078.
Quade, J., C. N. Garzione, and J. M. Eiler (2007), Paleoelevation reconstruction using pedogenic carbonates, *Rev. Mineral. Geochem.*, *66*(1), 53–87, doi:10.2138/rmg.2007.66.3.
Rasmussen, K. L., S. L. Choi, M. D. Zuluaga, and R. A. Houze Jr. (2013), TRMM precipitation bias in extreme storms in South America, *Geophys. Res. Lett.*, *40*, 3457–3461, doi:10.1002/grl.50651.
Rindsberger, M., M. Magaritz, I. Carmi, and D. Gilad (1983), The relation between air-mass trajectories and the water isotope composition of rain in the Mediterranean-Sea area, *Geophys. Res. Lett.*, *10*(1), 43–46, doi:10.1029/GL010i001p00043.
Risi, C., S. Bony, and F. Vimeux (2008), Influence of convective processes on the isotopic composition (δ^{18}O and δD) of precipitation and water vapor in the tropics: 2. Physical interpretation of the amount effect, *J. Geophys. Res.*, *113*, D19306, doi:10.1029/2008JD009943.
Rodwell, M. J., and B. J. Hoskins (2001), Subtropical anticyclones and summer monsoons, *J. Clim.*, *14*(15), 3192–3211.
Rohrmann, A., M. R. Strecker, B. Bookhagen, A. Mulch, D. Sachse, H. Pingel, R. N. Alonso, T. F. Schildgen, and C. Montero (2014), Can stable isotopes ride out the storms? The role of convection for water isotopes in models, records, and paleoaltimetry studies in the central Andes, *Earth Planet. Sci. Lett.*, *407*, 187–195, doi:10.1016/j.epsl.2014.09.021.
Ronchail, J., and R. Gallaire (2006), ENSO and rainfall along the Zongo valley (Bolivia) from the Altiplano to the Amazon basin, *Int. J. Climatol.*, *26*(9), 1223–1236, doi:10.1002/joc.1296.
Ronchail, J., L. Bourrel, G. Cochonneau, P. Vauchel, L. Phillips, A. Castro, J.-L. Guyot, and E. de Oliveira (2005), Inundations in the Mamoré basin (south-western Amazon—Bolivia) and sea-surface temperature in the Pacific and Atlantic Oceans, *J. Hydrol.*, *302*(1–4), 223–238, doi:10.1016/j.jhydrol.2004.07.005.
Rowley, D. B., and C. N. Garzione (2007), Stable isotope-based paleoaltimetry, *Annu. Rev. Earth Planet. Sci.*, *35*(1), 463–508, doi:10.1146/annurev.earth.35.031306.140155.
Rozanski, K., L. Araguas-Araguas, and R. Gonfiantini (1993), Isotopic patterns in modern global precipitation, in *Climate Change in Continental Isotopic Records*, edited by P. K. Swart et al., pp. 1–36, AGU, Washington, D. C.
Samuels-Crow, K. E., J. Galewsky, D. R. Hardy, Z. D. Sharp, J. Worden, and C. Braun (2014a), Upwind convective influences on the isotopic composition of atmospheric water vapor over the tropical Andes, *J. Geophys. Res. Atmos.*, *119*, 7051–7063, doi:10.1002/2014JD021487.
Samuels-Crow, K. E., J. Galewsky, Z. D. Sharp, and K. J. Dennis (2014b), Deuterium excess in subtropical free troposphere water vapor: Continuous measurements from the Chajnantor Plateau, northern Chile, *Geophys. Res. Lett.*, *41*, 8652–8659, doi:10.1002/2014GL062302.
Saylor, J. E., and B. K. Horton (2014), Nonuniform surface uplift of the Andean plateau revealed by deuterium isotopes in Miocene volcanic glass from southern Peru, *Earth Planet. Sci. Lett.*, *387*(C), 120–131, doi:10.1016/j.epsl.2013.11.015.
Scholl, M. A., S. E. Ingebritsen, C. J. Janik, and J. P. Kauahikaua (1996), Use of precipitation and groundwater isotopes to interpret regional hydrology on a tropical volcanic island: Kilauea volcano area, Hawaii, *Water. Resour. Res.*, *32*(12), 3525–3537, doi:10.1029/95WR02837.
Siegenthaler, U., and H. Oeschger (1980), Correlation of ^{18}O in precipitation with temperature and altitude, *Nature*, *285*, 314–317.
Silvestri, G. E. (2004), El Niño signal variability in the precipitation over southeastern South America during austral summer, *Geophys. Res. Lett.*, *31*, L18206, doi:10.1029/2004GL020590.
Smith, T. M., R. W. Reynolds, T. C. Peterson, and J. Lawrimore (2008), Improvements to NOAA's historical merged land–ocean surface temperature analysis (1880–2006), *J. Clim.*, *21*(10), 2283–2296, doi:10.1175/2007JCLI2100.1.
Strong, M., Z. D. Sharp, and D. S. Gutzler (2007), Diagnosing moisture transport using D/H ratios of water vapor, *Geophys. Res. Lett.*, *34*, L03404, doi:10.1029/2006GL028307.
Sturm, C., G. Hoffmann, and B. Langmann (2007), Simulation of the stable water isotopes in precipitation over South America: Comparing regional to global circulation models, *J. Clim.*, *20*(15), 3730–3750.
Takahashi, K., and D. S. Battisti (2007), Processes Controlling the Mean Tropical Pacific Precipitation Pattern. Part I: The Andes and the Eastern Pacific ITCZ, *J. Clim.*, *20*(14), 3434–3451, doi:10.1175/JCLI4198.1.
Thompson, L. G., E. Mosley-Thompson, and B. M. Arnao (1984), El Niño-Southern Oscillation events recorded in the stratigraphy of the tropical Quelccaya ice cap, Peru, *Science*, *226*(4670), 50–53.
Thompson, L. G., M. E. Davis, E. Mosley-Thompson, T. A. Sowers, K. A. Henderson, V. S. Zagorodnov, P.-N. Lin, V. N. Mikhalenko, R. K. Campen, and J. F. Bolzan (1998), A 25,000-year tropical climate history from Bolivian ice cores, *Science*, *282*(5395), 1858–1864, doi:10.1126/science.282.5395.1858.
Thompson, L. G., E. Mosley-Thompson, M. E. Davis, V. S. Zagorodnov, I. M. Howat, V. N. Mikhalenko, and P.-N. Lin (2013), Annually resolved ice core records of tropical climate variability over the past ~1800 years, *Science*, *340*(6135), 945–950, doi:10.1126/science.1234210.
Uemura, R., Y. Matsui, K. Yoshimura, H. Motoyama, and N. Yoshida (2008), Evidence of deuterium excess in water vapor as an indicator of ocean surface conditions, *J. Geophys. Res.*, *113*, D19114, doi:10.1029/2008JD010209.

Vimeux, F., R. Gallaire, S. Bony, G. Hoffmann, and J. C. H. Chiang (2005), What are the climate controls on δD in precipitation in the Zongo Valley (Bolivia)? Implications for the Illimani ice core interpretation, *Earth Planet. Sci. Lett.*, *240*(2), 205–220, doi:10.1016/j.epsl.2005.09.031.

Vimeux, F., P. Ginot, M. Schwikowski, M. Vuille, G. Hoffmann, L. Thompson, and U. Schotterer (2009), Climate variability during the last 1000 years inferred from Andean ice cores: A review of methodology and recent results, palaeogeography, palaeoclimatology, *Palaeoecology*, *281*(3–4), 229–241, doi:10.1016/j.palaeo.2008.03.054.

Vimeux, F., G. Tremoy, C. Risi, and R. Gallaire (2011), A strong control of the South American SeeSaw on the intra-seasonal variability of the isotopic composition of precipitation in the Bolivian Andes, *Earth Planet. Sci. Lett.*, *307*(1–2), 47–58, doi:10.1016/j.epsl.2011.04.031.

Vuille, M. (1999), Atmospheric circulation over the Bolivian Altiplano during dry and wet periods and extreme phases of the Southern Oscillation, *Int. J. Climatol.*, *19*, 1579–1600.

Vuille, M., and M. Werner (2005), Stable isotopes in precipitation recording South American summer monsoon and ENSO variability: Observations and model results, *Clim. Dyn.*, *25*(4), 401–413, doi:10.1007/s00382-005-0049-9.

Vuille, M., D. R. Hardy, C. Braun, F. Keimig, and R. S. Bradley (1998), Atmospheric circulation anomalies associated with 1996/1997 summer precipitation events on Sajama Ice Cap, Bolivia, *J. Geophys. Res.*, *103*(D10), 11,191–11,204, doi:10.1029/98JD00681.

Vuille, M., R. S. Bradley, and F. Keimig (2000), Interannual climate variability in the Central Andes and its relation to tropical Pacific and Atlantic forcing, *J. Geophys. Res.*, *105*(D10), 12,447–12,460, doi:10.1029/2000JD900134.

Vuille, M., R. S. Bradley, M. Werner, R. Healy, and F. Keimig (2003a), Modeling δ^{18}O in precipitation over the tropical Americas: 1. Interannual variability and climatic controls, *J. Geophys. Res.*, *108*(D6), 4174, doi:10.1029/2001JD002038.

Vuille, M., R. S. Bradley, R. Healy, M. Werner, D. R. Hardy, L. G. Thompson, and F. Keimig (2003b), Modeling δ^{18}O in precipitation over the tropical Americas: 2. Simulation of the stable isotope signal in Andean ice cores, *J. Geophys. Res.*, *108*(D6), 4175–4192, doi:10.1029/2001JD002039.

Vuille, M., S. J. Burns, B. L. Taylor, F. W. Cruz, B. W. Bird, L. C. Kanner, H. Cheng, and V. F. Novello (2012), A review of the South American monsoon history as recorded in stable isotopic proxies over the past two millennia, *Clim. Past*, *8*(4), 1309–1321, doi:10.5194/cp-8-1309-2012.

Wang, X., A. Auler, R. Edwards, H. Cheng, P. Cristalli, P. Smart, D. Richards, and C. Shen (2004), Wet periods in northeastern Brazil over the past 210 kyr linked to distant climate anomalies, *Nature*, *432*(7018), 740–743, doi:10.1038/nature03067.

West, A. G., G. R. Goldsmith, I. Matimati, and T. E. Dawson (2011), Spectral analysis software improves confidence in plant and soil water stable isotope analyses performed by isotope ratio infrared spectroscopy (IRIS), *Rapid Commun. Mass Spectrom.*, *25*(16), 2268–2274, doi:10.1002/rcm.5126.

WMO/IAEA (2013), *Global Network of Isotopes in Precipitation*, The GNIP Database. [Available at http://www.iaea.org/water, http://www-naweb.iaea.org/napc/ih/IHS_resources_gnip.html, Accessed 6 September 2013.]

Xie, P. P., and P. A. Arkin (1998), Global monthly precipitation estimates from satellite-observed outgoing longwave radiation, *J. Clim.*, *11*(2), 137–164.

Zhang, G. J., and N. A. McFarlane (1995), Sensitivity of climate simulations to the parameterization of cumulus convection in the Canadian climate centre general circulation model, *Atmos. Ocean*, *33*(3), 407–446, doi:10.1080/07055900.1995.9649539.